AD_____

Award Number: W81XWH-18-1-0519

TITLE: Early Detection of Castration-Resistant Prostate Cancer by Assessing Interactions between Circulating Tumor Cells and Accompanying Immune Cells

PRINCIPAL INVESTIGATOR: Tim H. Huang, Ph.D.

CONTRACTING ORGANIZATION:

University of Texas Health Science Center at San Antonio, San Antonio, TX 78245

REPORT DATE: September 2019

TYPE OF REPORT: Annual

PREPARED FOR:
DEPARTMENT OF THE ARMY US ARMY MEDICAL RESEARCH ACQUISITION ACTIVITY 820 CHANDLER STREET FORT DETRICK MD 21702-5014

DISTRIBUTION STATEMENT:

x Approved for public release; distribution unlimited

REPORT DOCUMENTATION PAGE

Form Approved
OMB No. 0704-0188

1. REPORT DATE *(DD-MM-YYYY)*	2. REPORT TYPE	3. DATES COVERED *(From - To)*
Sept /2019	Annual	15 Aug 2018 - 14 Aug 2019

4. TITLE AND SUBTITLE

Early Detection of Castration-Resistant Prostate Cancer by Assessing Interactions Between Circulating Tumor Cells and Accompanying Immune Cells

5a. CONTRACT NUMBER

5b. GRANT NUMBER
W81XWH-18-1-0519

5c. PROGRAM ELEMENT NUMBER

6. AUTHOR(S)
Huang, Tim H

Gaczynska, Maria

Osmulski, Pawel A.

5d. PROJECT NUMBER

5e. TASK NUMBER

5f. WORK UNIT NUMBER

7. PERFORMING ORGANIZATION NAME(S) AND ADDRESS(ES)

The University of Texas Health Science Center at San Antonio
Office of Sponsored Programs
7703 Floyd Curl Drive, Mail Code 7828
San Antonio, Texas 78229-3900

8. PERFORMING ORGANIZATION REPORT NUMBER

9. SPONSORING / MONITORING AGENCY NAME(S) AND ADDRESS(ES)
U.S. Army Medical Research
And Material Command
Fort Detrick, Maryland
21702-5012

10. SPONSOR/MONITOR'S ACRONYM(S)

11. SPONSOR/MONITOR'S REPORT NUMBER(S)

12. DISTRIBUTION / AVAILABILITY STATEMENT

Approved for public release; distribution unlimited

13. SUPPLEMENTARY NOTES

14. ABSTRACT
Prostate cancer (PCa) is the most frequently diagnosed cancer in men. In majority of "castration sensitive" patients proliferation of cancer cells can be attenuated by the androgen deprivation therapy (ADT). Unfortunately, many patients develop "castration resistance" (CR) followed by metastatic spread. For effective second-line therapy the resistance needs to be detected early. We postulate that mechanical and immunochemical profiling of blood-isolated "seeds of metastasis" (circulating tumor cells; CTCs) points at CTCs aggressiveness indicating risk of CR. Our specific aims call for determining the role of (1) epithelial-mesenchymal transition (EMT) and (2) interactions with circulating macrophages in survival-promoting mechanical fitness of CTCs. Based on profiling of CTCs and model cultured cells we plan to (3) construct a predictive model for early CR detection. In this reporting period we met the goal for accrual of patients starting ADT and for profiling of patient-isolated CTCs. Consistent with our hypothesis, we detected unique invasiveness-indicating hybrid EMT features in patients' CTCs and model PCa cells co-cultured with model macrophages. To improve fidelity of our cell culture model of acquired aggressiveness, we introduced circulation-simulating fluid shear stress, with very promising initial results. The outcomes include a manuscript submitted and a poster presented with the abstract published.

15. SUBJECT TERMS
androgen deprivation therapy, atomic force microscopy, castration resistance, castration sensitivity, circulating tumor cells, cultured cells, epithelial-mesenchymal transition

16. SECURITY CLASSIFICATION OF:			17. LIMITATION OF ABSTRACT	18. NUMBER OF PAGES	19a. NAME OF RESPONSIBLE PERSON
U					USAMRMC
a. REPORT	b. ABSTRACT	c. THIS PAGE	UU	76	19b. TELEPHONE NUMBER *(include area code)*
U	U	U			

Table of Contents

Page

1. Introduction

Prostate cancer (PCa) is the most frequently diagnosed cancer in men. In majority of "castration sensitive" patients proliferation of cancer cells depends on supply of androgen and can be attenuated by the androgen deprivation therapy (ADT). Unfortunately, many patients develop "castration resistance" (CR), when the tumor growth and metastatic spread continue despite ADT. For effective second-line therapy that saves lives and improves life quality the resistance needs to be detected early. To reach the goal of early detection we propose to test properties of rare cells that are responsible for spreading metastasis. These circulating tumor cells (CTCs) are shed from the primary tumor or metastatic lesions and can be isolated from the standard blood sample are considered "seeds of metastasis". Majority of CTCs die, however the surviving "aggressive" cells travel with blood, undergo epithelial-to-mesenchymal transition (EMT), extravasate and start secondary tumor growth in distant organs. Since CTCs have to escape from the tumor and then survive in the turbulent blood stream, they have to be mechanically fit. Indeed, we found in retrospective studies that CTCs obtained from CR patients are much softer, deformable and more adhesive than CTCs from CS patients. CTCs are often accompanied by innate immune cells, mostly macrophages. We found that interactions with macrophages of certain polarization may help CTCs to survive. We postulate that mechanical and immunochemical profiling of CTCs and co-purifying immune cells (tumor associated circulating cells; TACCs) provide clues about CTCs aggressiveness and the risk of CR. Our specific aims call for determining the role of (1) epithelial-mesenchymal transition and (2) interactions with circulating macrophages in survival-promoting mechanical fitness of CTCs. Combining the cell culture studies with profiling of CTCs will lead to (3) construction of predictive model for early CR detection. According to the Statement of Work (SOW), our goals for this reporting period (months 1-12) were: (a) accrual of about half of required number of patients starting ADT; (b) isolation, enumeration, mechanical and molecular profiling as well as immunochemical characterization of TACCs from these patients' blood; (c) performing a subset of experiments aiming at recapitulation of EMT in cell culture model; the experiments include mechanical and molecular profiling of control and EMT-induced cells.

2. Keywords

androgen deprivation therapy
atomic force microscopy
castration resistance
castration sensitivity
circulating tumor cells
cultured cells
epithelial-mesenchymal transition
gene expression
immune cells
immunostaining
liquid biopsy
macrophage
macrophage polarization
mechanical phenotype
metastasis
prostate cancer
protein expression
single-cell profiling

3. Accomplishments

3.1 The major goals for this reporting period (months 1-12) and ahead-of-schedule tasks, as stated in the approved SOW, with % of completion

---

Research-Specific Tasks:

Specific Aim 1: We will determine the role of epithelial to mesenchymal transition in mechanical fitness of CTCs.	**Months**	**Participants**	**% completion (mo. 1-12)**
Major Task 1: Recruit post-castration metastatic PCa patients experiencing biochemical recurrence and starting first line ADT	4-26	Drs. Huang, Liss	55
Major Task 2: Isolate and immunostain TACCs from the samples of blood drawn from the patients right before the start of ADT (70 patients, time t0), enumerate CTCs.	4-28		45
Subtask 1: Perform microfiltration, immunostain the cells. Device for cell isolation: ScreenCell CC ha (ScreenCell)	4-26	Drs. Osmulski, Gaczynska, Chen,	55
Subtask 2: Enumerate the isolated and immunostained CTCs and classify them as $EpCAM^+$ or EMT-CTCs according to surface antigen expression.	4-26	Drs. Gaczynska, Osmulski	15
Major Task 3: Collect multiparameter nanomechanical and morphological data on individual isolated CTCs using PeakForce Quantitative Nanomechanics (PF QNM) AFM imaging.	4-30		35
Subtask 1: Collect the AFM images.	4-26	Drs. Osmulski, Gaczynska	55
Subtask 2: Perform image and data analysis on the collected AFM images.	4-30	Drs. Osmulski, Gaczynska	15
Major Task 4: Perform the gene expression analysis on CTCs.	4-26		15

Major Task 5: Recapitulate EMT in cell culture model	6-24		30
Subtask 1: Culture 22Rv1 and DU145 cells (source: ATCC) according to ATCC recommendations. Induce EMT by treatment with TGF-β. Perform mechanical phenotyping of selected cultured cells.	6-18	Drs. Osmulski, Gaczynska	50
Subtask 2: Perform gene expression analysis of cultured cells that were mechanically phenotyped.	6-18	Dr. Chen	30
Specific Aim 2: We will define the role of CTC-macrophage interactions in mechanical fitness of CTCs.			
Major Task 6: Define the functional composition of macrophage population in TACCs preparations isolated from patients' blood.	1-26		20
Subtask 1: Enumerate and classify non-CTC patient-isolated TACCs according to immunostaining, enumerate CTC-immune cell clusters.	1-24	Drs. Gaczynska, Osmulski	20
Subtask 2: Perform the gene expression analysis on randomly selected cells (up to 30) bearing immune cell markers.	1-32	Dr. Chen	0
Major Task 7: Recapitulate the interactions of model "CTCs" (prostate cancer cell lines) cultured with polarized macrophages.	12-30		20 (ahead)
Subtask 1: Co-culture 22Rv1 and DU145 cells with model macrophages derived from U937 cells (source: ATCC). Determine rates of growth of co-cultured cells, enumerate cell clusters.	12-24	Drs. Gaczynska, Osmulski	30 (ahead)
Subtask 2: Perform mechanical phenotyping of selected cultured cells, free or in clusters.	12-24	Drs. Osmulski, Gaczynska	30 (ahead)
Subtask 3: Perform the gene expression analysis on model CTCs and macrophages.	12-30	Dr. Chen	10 (ahead)
Specific Aim 3. We will construct a model for patients' stratification predicting the risk of castration resistance based on the mechanical fitness of CTCs.			
Major Task 8: Collect mechanical and immunocytochemical properties of TACCs	6-30		

isolated at time t1 (6 months or at failure)			15
Subtask 1: Perform microfiltration, immunostain the cells, enumerate as for t0.	6-30	Drs. Gaczynska, Osmulski	15
Subtask 2: Perform mechanical profiling of CTCs at time t1, perform image and data analysis on the collected AFM images as for t0.	6-30	Drs. Osmulski, Gaczynska	10
Subtask 3: Compare clinical and biophysical/gene expression data at t1	6-30	Drs. Huang, Liss, Gelfond, Osmulski, Gaczynska	15

3.2 Specific accomplishments under the Major Tasks listed above:

3.2.1 Specific Aim 1, Major Task 1

We planned to accrue a total of 70 metastatic prostate cancer patients starting first-line ADT. During the first 12 months of the project duration we accrued a total of 38 patients (54%). The accrual proceeds as planned and we do not anticipate problems with accrual of the remaining 34 patients in the next 14 months.

Table 1 presents the accrual numbers, with information on data collected, relevant for Major Tasks 1-4, 6 and 8.

Number	Total	1st visit (t0)	Two visits (t0 and t1)
Patients (PTs) accrued	**38**	**27**	**11**
Filters with TACCs Collected for Mechanical and Immunochemical Phenotyping	49	27	22
TACCs Retained on Filters (approximately)	7000	4000	3000
Mechanically Phenotyped PT Samples	49	27	22
PT Samples with Mechanical Phenotype Analyzed	20	6	14
CTCs with Mechanical Phenotype Collected	784	432	352
CTCs with Mechanical Phenotype Analyzed	304	102	202
Immunostaining Performed and Cell Images Collected for PT Samples	49	27	22
Total Immunostaining Images Collected	940	500	440
PT Samples with CTC Enumeration Completed	34	24	10
PT Samples with TACCs Enumeration Completed	14	4	10
PT Samples with Cells Collected for Gene and Protein Expression Analysis	49	27	22
PT Samples with CTCs analyzed by single-cell transcriptomics	10	10	0
CTCs analyzed by single-cell transcriptomics	136	136	0

3.2.2 Specific Aim 1, Major Task 2

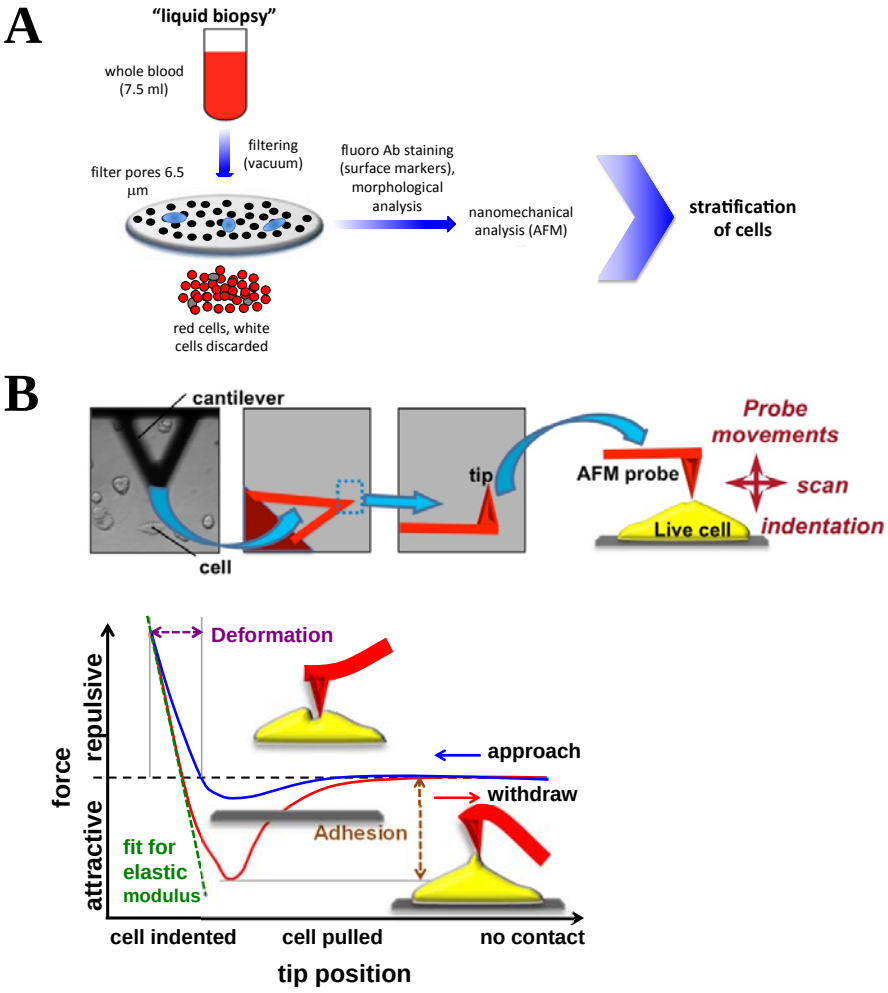

Figure 1 Processing of liquid biopsy samples from prostate cancer patients.
A: isolation of large tumor associated circulating cells (TACCs). A separate filter is used to collect additional TACCs for gene and protein expression analysis. **B**: nanomechanical profiling: a small silicon probe on a cantilever "pokes" the cell with extremely small (nanoNewton-scale) force to collect "force curves" used to extract precise numerical data on elasticity (reversible change of shape), deformability (reversible and non-reversible, nondestructive change of shape) and adhesiveness.

For all blood samples we collected filters with retained cells and images of immunostained TACCs (*Subtask 1*). The patient's blood samples were processed within two hours from phlebothomy, as planned. Processing included microfiltration with the ScreenCell device retaining all cells that do not pass through 6.5 µm pores randomly distributed in the filters. The filters are formulated for cells' adherence, important to hold cells for AFM profiling. The cells still attached to the filters are subjected to nanomechanical imaging. The methods of processing and AFM imaging are presented above in **Figure 1.**

To date, we fully enumerated and classified TACCs for about 30% of collected samples (*Subtask 2*). See **Table 1** for details. **Figure 2** displays examples of diverse TACCs collected on the filters. **Figure 3** presents partition of TACCs in 13 of the already processed patient samples.

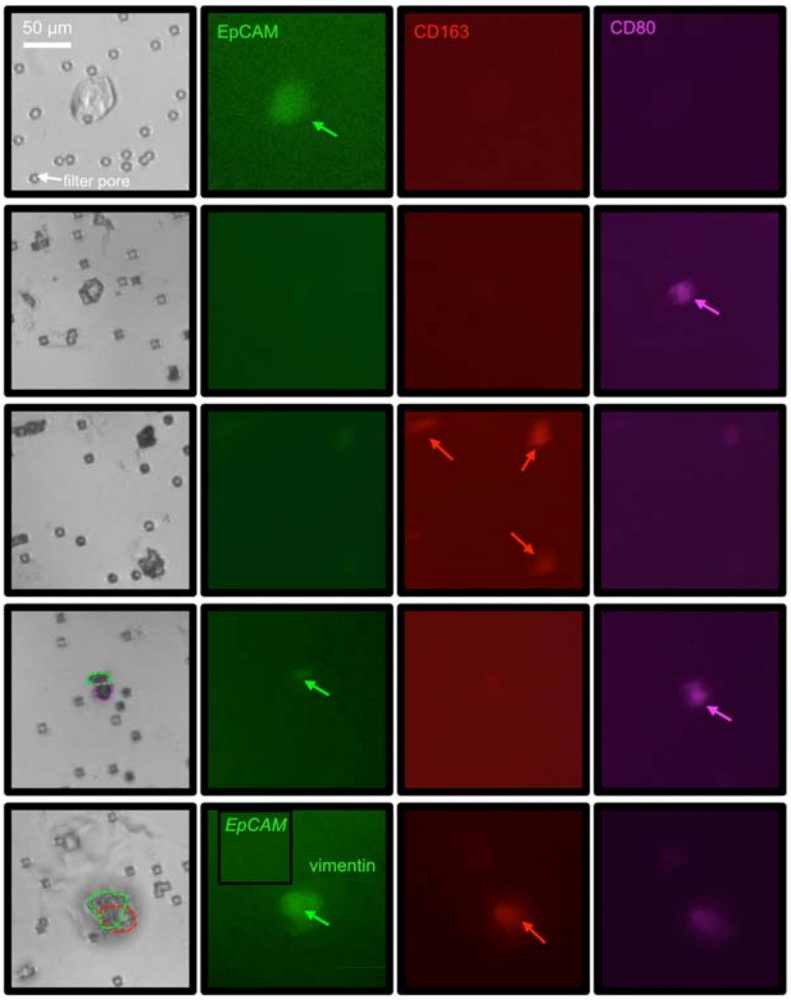

Figure 2 CTCs and macrophage-like immune cells co-purify during microfiltration of blood of prostate cancer patients. A gallery of tumor associated circulating cells on a filter stained with antibodies specific for surface antigen biomarkers of epithelial-like cells ($EpCAM^+$), cells undergoing EMT ($vimentin^+$) and cells resembling macrophages of distinct polarization. From top to bottom: typical $EpCAM^+$ CTC, cells positive for markers of M2-like macrophages ($CD163^+$/weak or no CD80) or M1-like macrophages ($CD80^+$), pair of $EpCAM^+$ CTC and M1-like macrophage, cluster of EMT-undergoing CTCs paired with M2-like macrophage. Insert: the cell was treated first with fluorescent anti-EpCAM antibodies; the cell-covering area is shown.

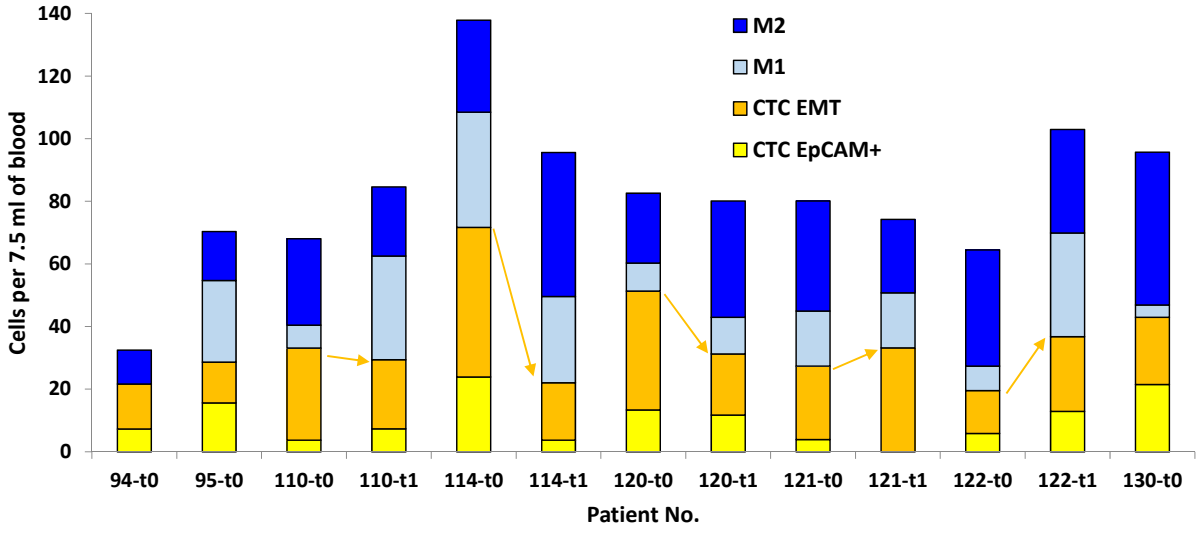

Figure 3 Partition of CTCs and macrophage-like immune cells isolated from the blood of eight patients. Four classes of TACCs are distinguished: typical CTCs (EpCAM^{+}), EMT-undergoing CTCs (EpCAM^{-}/vimentin^{+}), M1-like macrophages (CD80^{+}), M2-like macrophages (CD163^{+}/CD80^{-} or $^{+}$). Differences in EMT-CTC partitions between t0 and t1 are marked by arrows.

3.2.3 Specific Aim 1, Major Task 3

Mechanical phenotypes of single CTCs were collected with atomic force microscopy (AFM) PeakForce Quantitative Nanomechanical mode for all collected samples immediately after microfiltration, as planned (*Subtask 1*). As for now, the collected data are fully processed and analyzed for 11 collected samples (*Subtask 2*; see **Table 1** for details). **Figure 4** presents examples of AFM images of CTCs and a pair of CTC and macrophage. processed samples.

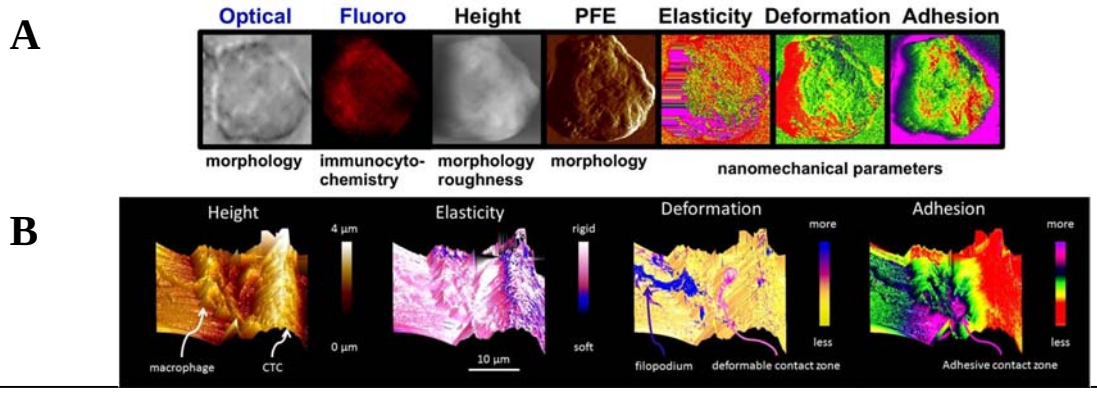

Figure 4 PeakForce Quantitative Nanomechanics (PF-QNM) AFM imaging delivers nanomechanical phenotype o circulating tumor cells. A. An example of CTC: the same cell is characterized by immunofluorescence as well as morphological and nanomechanical parameters. **B**. Nanomechanical phenotype of a pair of CTC and macrophage points at differences between them and highlights a unique set of parameters at the cell-cell contact zone (pseudo-3D rendering).

Figures 5 and 6 below display nanomechanical phenotype parameters for the 20 so-far processed patient samples, relevant also for *Specific Aim 2, Major Task 8*.

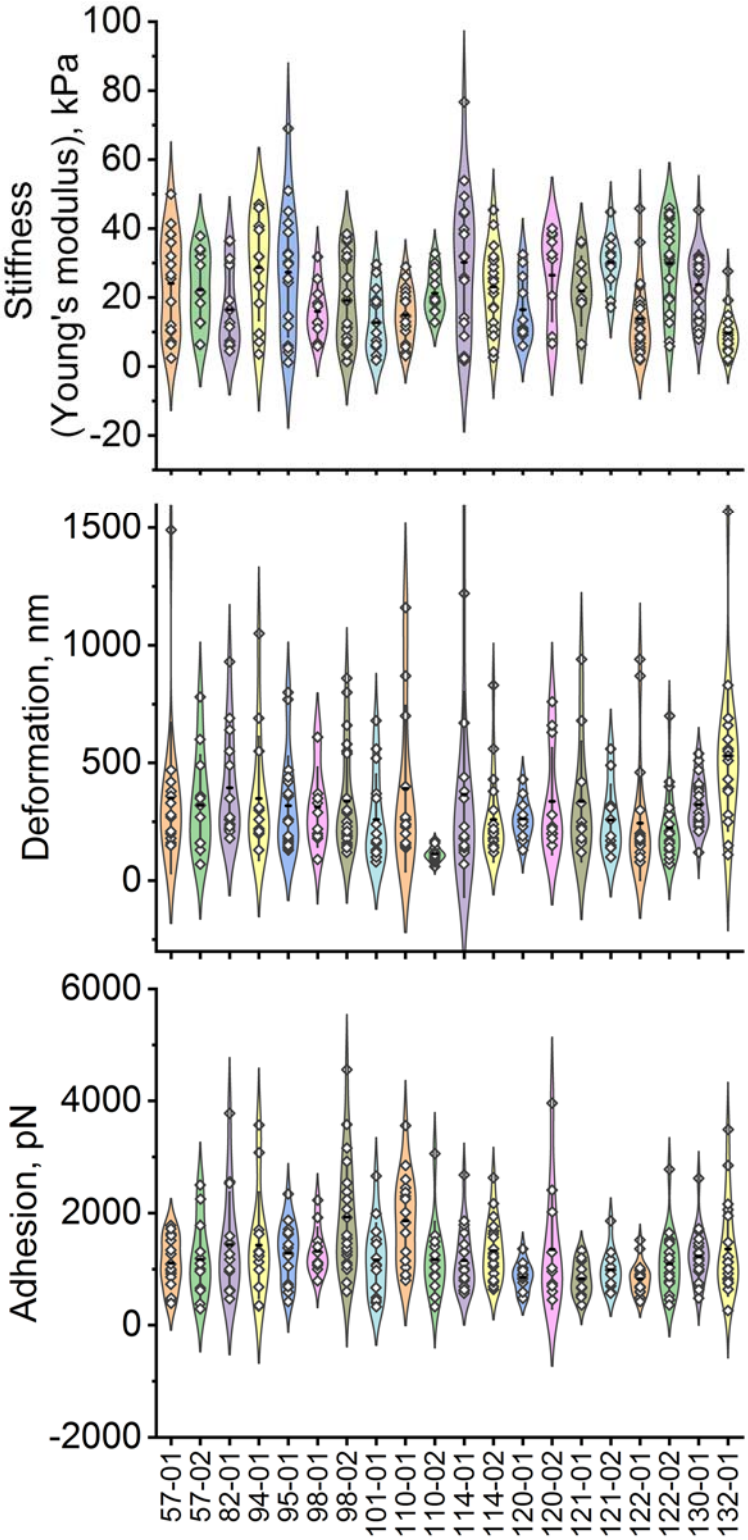

Figure 5 Mechanical phenotype parameters determined for randomly selected CTCs isolated from 20 patient samples. Each dot represents a single CTC. Note the diversity of phenotypes and the (expected) large spread of some values. According to our previous works, less stiff, more deformable and more adhesive CTCs should be considered more aggressive. Phenotypes change between t0 ("-1") and t1 ("-2") visits in all four analyzed patients. For example, increasing Young modulus (stiffness), decreasing deformability and decreasing adhesion in CTCs of patient 110 indicate a good prognosis for first line ADT.

Apparent mechanical phenotype	class	Average			Range					
		Deformation	Stiffness	Adhesion	Deformation		Stiffness		Adhesion	
		nm	kPa	pN	min	max	min	max	min	max
v. hard, non- sticky	1	214.3	35.0	924.4	94.2	334.3	26.0	44.0	594.9	1253.9
hard, v. sticky	2	246.5	25.0	2478.8	128.6	364.4	14.1	35.8	1744.9	3212.8
v. soft, sticky	3	718.2	6.7	1414.4	421.2	1015.2	2.8	10.6	785.0	2043.8
soft, non-sticky	4	237.6	13.8	1029.2	127.2	348.1	7.8	19.8	611.9	1446.6

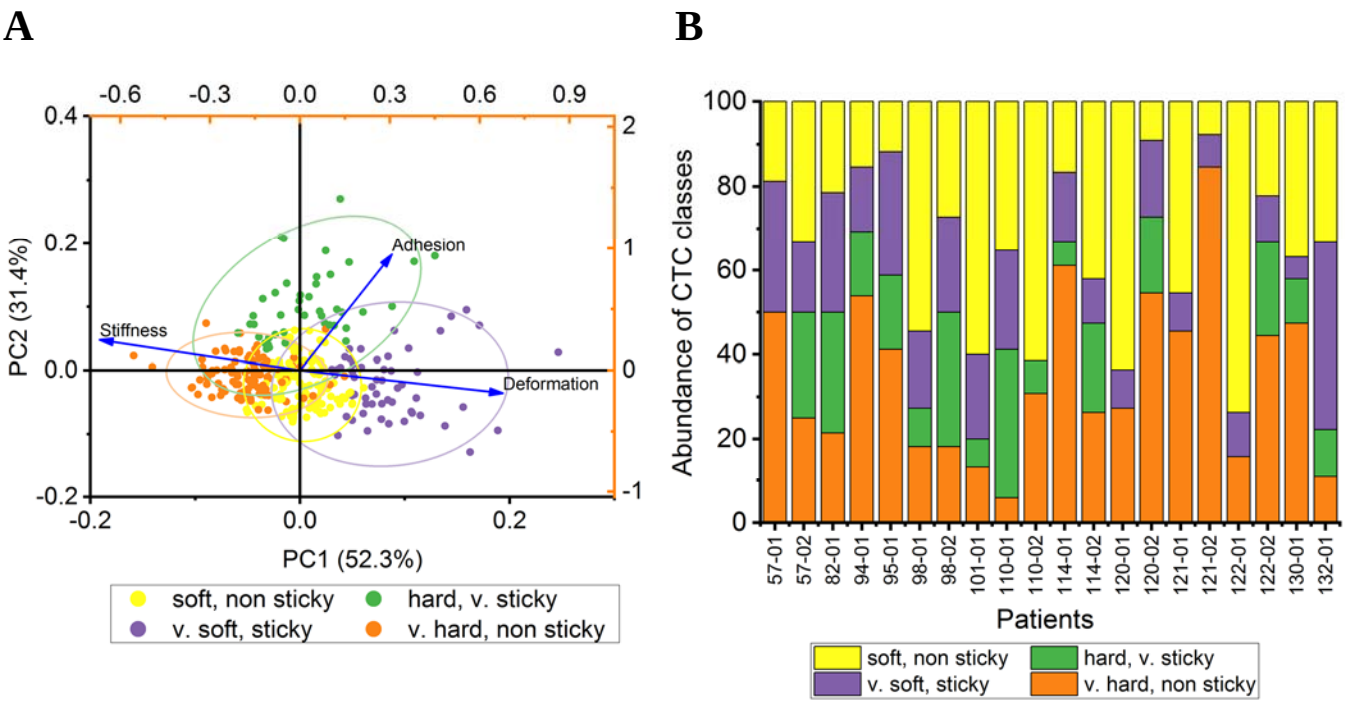

Figure 6 Phenotypical diversity of patient-isolated CTCs. The Table summarizes properties of mechanical phenotypes identified with clustering analysis. The ranges labelled in red enable unique classification of cells **A.** Principal component analysis (PCA) reveals the presence of four classes of cells with distinct mechanical phenotypes. Soft cells are considered the most invasive. Cell classes were identified with the unsupervised hierarchical clustering **B.** Abundance of the four classes of CTCs differs grossly between the patients and also between t0 and t1 for the same patient. For example, the population of invasive soft and sticky cells disappears at t1 in patient 110, a good prognosis. Note that for this patient the partition of likely-invasive EMT CTCs was lowered at t1 (Figure 3).

3.2.4 Specific Aim 1, Major Task 4

Sets of TACCs have been collected from all patients' samples (**Table 1)** and preserved (*Subtask 1*) for single cell gene expression analysis (CTCs) with the BioMark HD MX/HX and for multi-cell flow cytometry/mass spectrometry based protein expression analysis with the Helios CyTOF. So far, transcriptomic expression profiles were collected for 136 single CTCs (**Figure 7**).

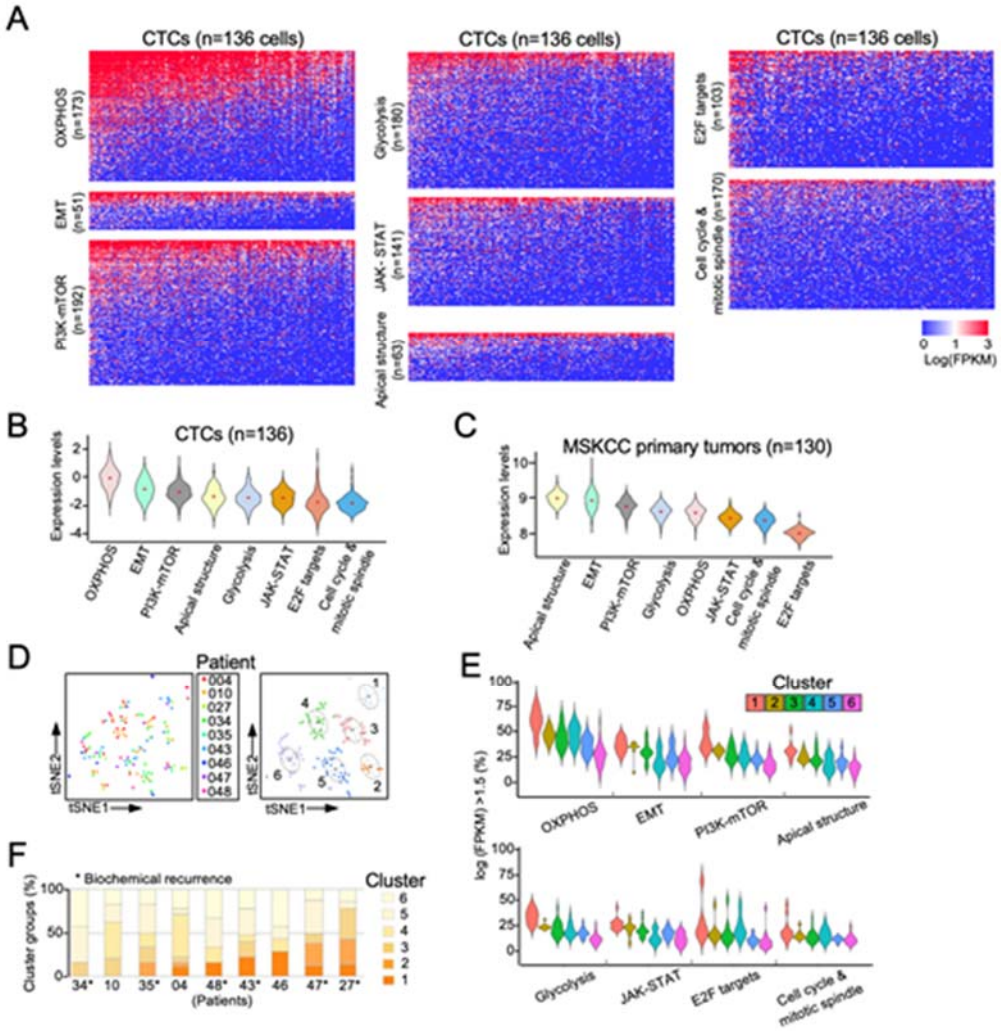

Figure 7 Heterogeneous Single-cell Expression Profiles of Eight Hallmark Pathways in CTCs. A. Transcriptomic heat maps of eight hallmark pathways. Genes with very low or no expression across cells in each pathway were excluded in the analysis. **B**. Ranking of the expression levels of the eight hallmark pathways in CTCs. **C**. Ranking of the expression levels of the eight hallmark pathways in 130 bulk prostate tumors in the cohort from MSKCC. **D**. Unsupervised clustering on 136 CTCs with t-SNE (left), and six clusters were identified in different colors (right) (see STAR Methods). **E**. Percentage of expressed genes (log FPKM > 1.5) in each hallmark pathway for the cells in each of the six clusters from (D). **F**. Percentage of the cells in each cluster per patient.

Importantly, we found upregulation of EMT related genes expression in CTCs, as compared with Memorial Sloan Kettering Cancer Center (MSKCC) cohort database of prostate tumor cells. See also **Appendix**: the manuscript submitted.

Since the single cells that are mechanically phenotyped are already characterized and classified for their surface marker expression by immunostaining (**Figure 2**), to extract maximum molecular information from the patients' samples we decided to collect additional sets of TACCs for single cell gene expression profiling and for multi-cell protein expression profiling with the exceptionally effective multi-parameter CyTOF analysis. An example of CyTOF – derived data for cultured cells is presented below in **Figure 11**. The patient-isolated cells are preserved and will be analyzed within the time period declared in SOW (up to month 26; *Subtask 2*).

3.2.5 Specific Aim 1, Major Task 5

In our search for methods of EMT induction in cultured prostate cancer cells serving as "model CTCs" we came upon an important preliminary finding: that cells subjected to fluid shear stress (FSS) imitating the conditions that CTCs endure in the circulation start to undergo a partial EMT and acquire a "mechanical fitness" phenotype promoting survival and aggressiveness. Interestingly, cultured cells with the most aggressive mechanical phenotype (**Figure 8A**) were best-survivors of FSS (**Figure 8B**). We performed mechanical phenotyping of control and FSS-subjected DU145 cells (*Subtask 1*). Interestingly, the cells display increased adhesiveness (**Figure 6C**), an epithelial-like trait that we found before connected to "aggressive" phenotype of CTCs. At the same time, we detected an increased expression of EMT markers such as vimentin in cultured cells subjected to FSS (**Figure 6D**). We probed the influence of FSS and the induction of hybrid EMT not only in DU145 cells, but also in 22Rv-1 and C4-2 cells, with consistent preliminary results. Expression of EMT-related proteins was probed for the control and FSS-subjected DU145 cells with CyTOF (*Subtask 2*). Since the experiment involved also a co-culture with immune cells, the data are presented below with *Major Task 7* in **Figure 9**.

We hypothesize that increased adhesiveness promotes clustering of CTCs to chaperone macrophages, and that the partial ("hybrid") EMT detected in model cells imitates this property.

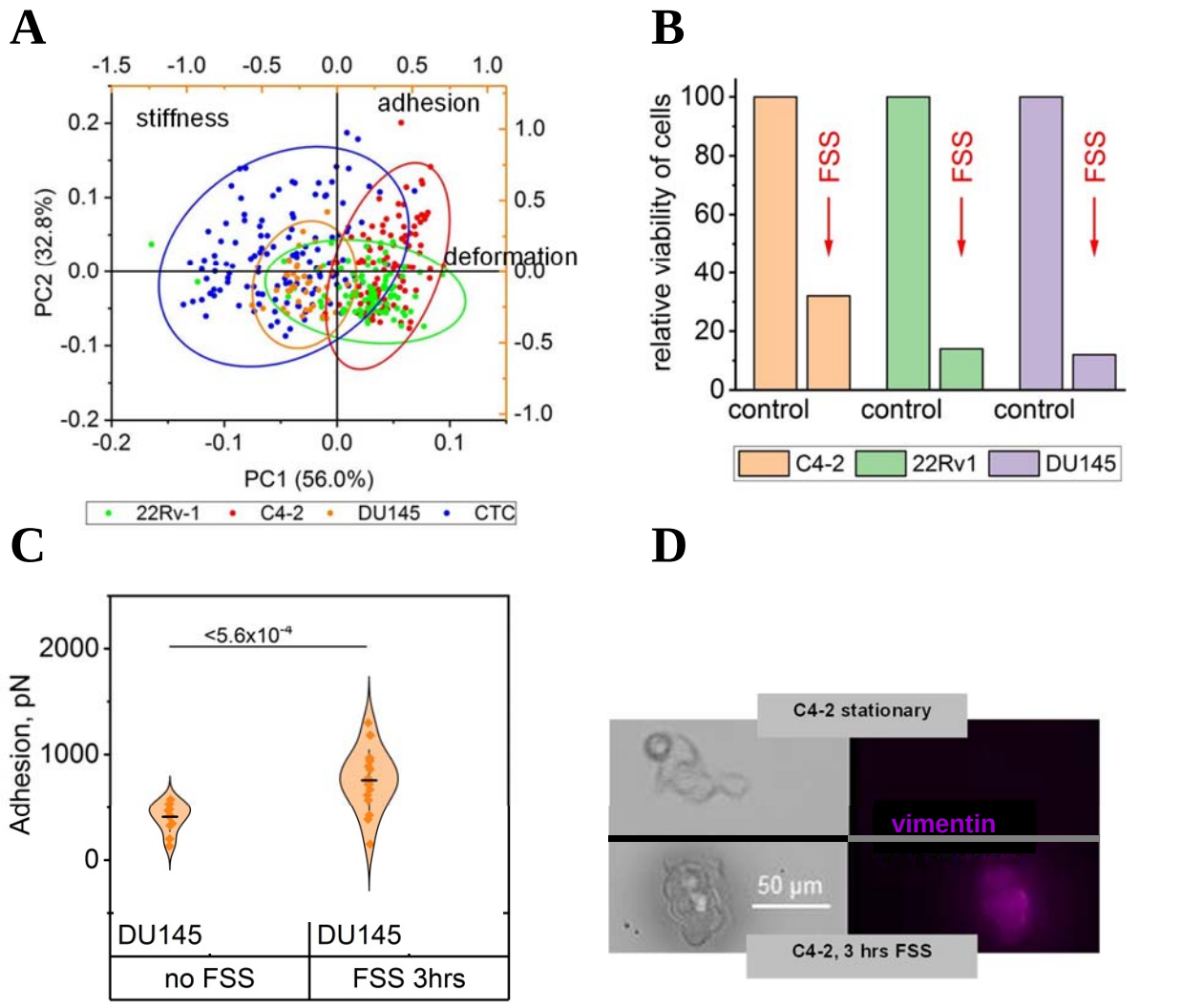

Figure 8 Mechanical phenotyping of model CTCs (cultured prostate cancer cells) indicates hybrid EMT as a hallmark of aggressive cells. A. Distinct cell lines present diverse yet well-defined mechanical phenotypes, as revealed by principal component analysis (PCA). The phenotype of DU145 cells is most similar to patient-isolated CTCs. Soft and adhesive C4-2 and 22Rv-1 cells display high mechanical fitness. **B**. Well-fit C4-2 cells are best survivors of FSS challenge. FSS: 7 dyn/cm^2; high vein-like/low capillary-like, applied for 3 hrs to cells in suspension. Viability: trypan blue exclusion. Viability was not affected after 1hr of FSS. Control: 0 hrs, identical with 3hrs without FSS. C. FSS-exposed surviving cells are more adhesive than non-stressed controls (epithelial trait), however they **D**. display upregulation of EMT marker vimentin. C4-2 cells are shown, upregulation was apparent in DU145 cells as well.

3.2.6 Specific Aim 2, Major Task 6

The immunostaining-based composition of macrophage population in TACCs (*Subtask 1*) was determined for selected samples, as stated in **Table 1** and demonstrated in **Figure 2**. The collected immunostaining images will be analyzed within the time period declared in SOW (up to month 24). Sets of TACCs are preserved for gene expression and protein expression analysis (*Subtask 2*) – see also *Major Task 4* above.

3.2.7 Specific Aim 2, Major Task 7

Recapitulation of interactions of model "CTCs" (prostate cancer cell lines) cultured with polarized macrophages has been planned for months 12-30, however we started some of the experiments ahead of time.

Figure 9 presents the scheme of co-culture experiments (*Subtask 1*).

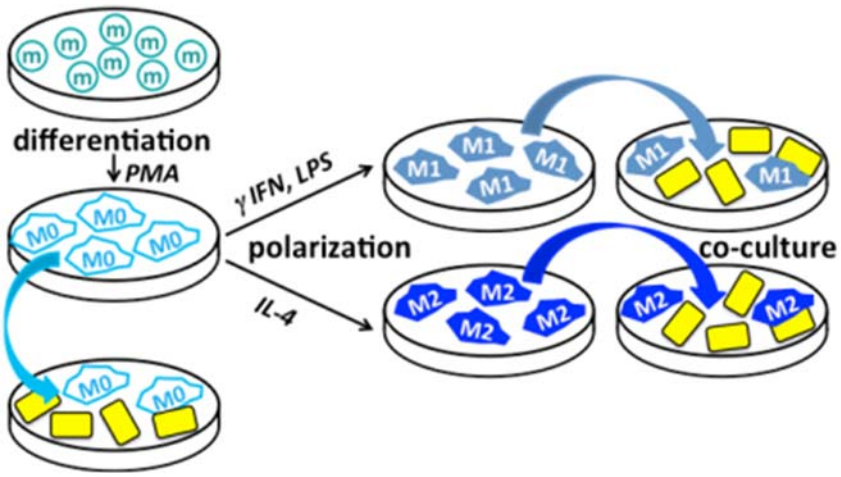

Figure 9 Cells from established prostate cancer lines were used as "model CTCs" (yellow rectangles) in co-culture experiments with model macrophages (blue shapes): human U937 cells differentiated (M0) and polarized into M1-like or M2-like macrophages.

Figure 10 below presents mechanical phenotypes of 22Rv-1 cells co-cultured with model macrophages differentiated and polarized from human U937 cultured monocytoidal cells (*Subtask 2*). Apparently, mechanical phenotypes of model CTCs shift toward higher mechanical fitness upon co-culture with chaperone M0 (differentiated, not committed) or M2 (anti-inflammatory - like polarization) model macrophages.

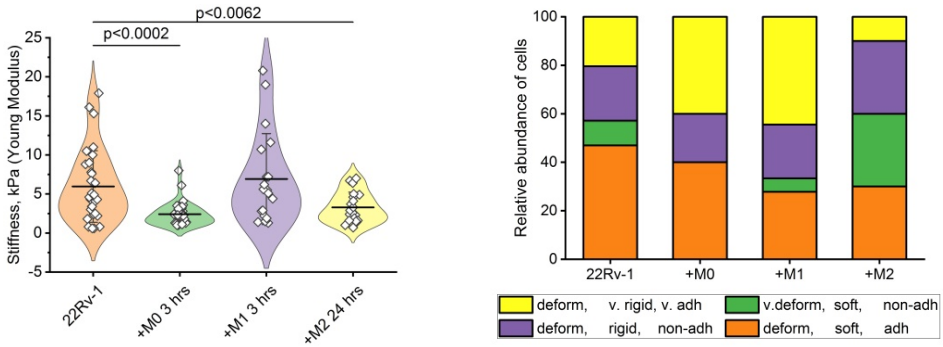

Figure 10 Mechanical phenotype of 22Rv-1 cells co-cultured with model M0 or M2 macrophages shifts toward higher aggressiveness.

Figure 11 presents expression of selected EMT-related marker proteins in DU145 cells subjected to FSS together with model monocytes (U937 cells) to simulate conditions encountered by CTCs in the bloodstream. Apparently, the cells display hybrid EMT.

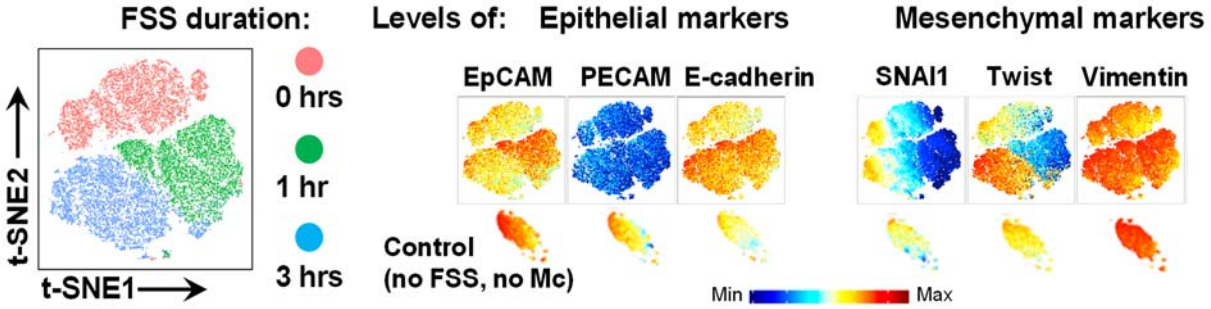

Figure 11. Subpopulations of "model CTCs" (DU145) co-cultured with "model monocytes"(U937) under FSS display hybrid EMT. GFP-DU145 were separated from Mcs in Cytobank and subjected to CyTOF with epithelial/mesenchymal panel of 16 antibodies. **Left:** t-SNE projections of treatments of DU145 cells. Each of 3 treatment-populations was further divided into six subpopulations. **Right:** Profiles of selected epithelial and mesenchymal markers under distinct duration of FSS. Bottom inserts: control DU145 in stationary culture. In generally, FSS and Mc-exposed cells display less epithelial phenotype than controls, however they escape a straightforward marker-based classification of EMT stage. Certain marker changes dependent on FSS duration, likely following stratification of cells' into a poorly fit population that would not survive the 3 hrs mark, and well-fit stress-adapted cells of mixed phenotype.

3.2.8 Specific Aim 2, Major Task 8

To date, samples were collected for 11 patients with both t0 and t1 visits. Data collection and analysis for *Subtasks 1 and 2* is in progress. See **Table 1** for details and **Figure 6** for preliminary conclusions.

3.3 Opportunities for training and professional development provided by the project:

- Dr. Chia-Nung Hung, Postdoctoral Fellow, is an enthusiastic young scientist devoted to single-cell molecular analysis of TACCs. He masters his training in gene and protein expression analysis and he generated part of data for *Major Tasks 2, 4, 6 and 7*. He is trained in nanomechanical profiling of single cells to complement his molecular biology skills with the biophysical component.

- Yusheng Qian, M.Sc., a PhD Graduate Student in Molecular Medicine joined the team most recently. Mr. Qian is well trained in molecular biology and he is currently learning single-cell biophysical techniques, most notably nanomechanical profiling and cell-cell interactions probing by AFM. He is mentored by Drs. Gaczynska and Osmulski and the prostate cancer model CTC project will constitute a core of his PhD thesis. He presented a poster "Nano-forces in the cellular world: probing interactions between model CTCs and macrophages by atomic force microscopy" on the Annual Molecular Medicine Departmental Retreat (August 2019).

3.4 Dissemination of the results to communities of interest:

- Poster presentation "Amplification-associated upregulation of genes involved in oxidative phosphorylation for disseminated prostate cancer cells." on the America Association for Cancer Research Annual Meeting, Atlanta, GA, March 2019; presenter: Dr. Lin (see Products).

- Poster presentation "Toxic relationship? Modelling Dynamics of Interactions between Circulating Tumor Cells and Macrophages in Metastatic Prostate Cancer" on the 10th Annual Frontiers of Translational Science Research Day, San Antonio, TX, May 2019, presenter: Dr. Osmulski. The event was attended by scientists from research institutions in San Antonio area, including UT Health, Mays Cancer Center, University of Texas at San Antonio, Southwest Research Institute, Southwest Foundation for Biomedical Research and Brooke Army Medical Center.

- Poster presentation "Nano-forces in the cellular world: probing interactions between model CTCs and macrophages by atomic force microscopy" on the Annual Molecular Medicine Departmental Retreat (August 2019). Presenter: Yusheng Qian.

- Presentation of the capabilities of the AFM technique on the Genome Repair Focus Group (UT Health SA, July 2019). Presentation included examples of CTC and model

CTC analysis by single-cell AFM and elicited great interest in the technique by colleagues from UT Health. Presenters: Drs. Gaczynska and Osmulski.

- Seminar presentation “From molecules to cells: the power of atomic force microscopy.”, Department of Biochemistry and Structural Biology, UT Health SA, September 2019. Presenters: Drs. Gaczynska and Osmulski.

3.5 Plans for the next reporting period:

We will continue the study following the Statement of Work for months 12-24.
- Majority of patients should be accrued.
- Mechanical and immunochemical profiles will be collected for all accrued patients.
- Gene expression data will be collected for selected CTCs.
- Majority of biophysical and molecular data will be analyzed.
- Initial attempts of statistical analysis of mechanical, immunochemical, molecular and clinical data will be performed.
- Co-culture experiments for model CTCs and macrophages will continue, including both “stationary” cultures and co-cultures including fluid shear stress.

4. Impact

4.1 Impact on the development of the principal discipline of the project.

The major findings in this reporting period are outlined below. The research is still in progress, however we believe that communicating these strong initial findings is warranted.

- Detection of hybrid epithelial-mesenchymal features in circulating tumor cells and in cell culture model of CTCs. Prostate cancer cells are epithelial-like. The most aggressive cancer cells are known to switch to mesenchymal-like phenotype, with increased motility (invasiveness). Our research, still in progress, indicates that the most invasive circulating tumor cells retain certain epithelial features, most notably high adhesiveness, as a special adaptation to mechanical stress endured in the bloodstream environment.
  Significance: the finding broadens the knowledge about the diversity of epithelial-to-mesenchymal transition processes that occur during normal development and differentiation but also accompanies cancerous spread. The knowledge will impact development of anti-metastasis therapies.

- Finding that fluid shear stress (FSS) simulating circulation-like conditions strongly affect survival of model CTCs. Cells that already display “mechanical fitness” phenotype, detected by atomic force microscopy profiling, are the most successful survivors. Moreover, phenotypical changes promoting mechanical fitness seem to be induced in model CTCs exposed to FSS.

Significance: targeting molecular mechanisms leading to "mechanically fit" phenotype may be a viable anti-metastatic strategy.

- Finding that model macrophages, especially non-polarized or of anti-inflammatory polarization promote "mechanically fit" phenotype in cultured cancer cells in a stationary co-culture model. The standard stationary co-culture may be considered a model for conditions on the tumor periphery, with relatively minor cell crowding and no significant interactions with stroma. Since cultured cancer cell lines are already relatively aggressive, the co-culture model is also useful for studying CTC-immune cells interactions.
  Significance: targeting anti-inflammatory macrophages may be a viable anti-metastatic strategy.

- Preliminary finding that co-culture with model monocytes strongly promote survival and promote mechanical fitness phenotype induction in FSS-exposed model CTCs. This is a potentially a very important observation, as monocytes have not been initially considered as "chaperones" in our model of CTC-immune cell interactions. We will pursue this exciting lead.
  Significance: targeting mechanisms leading to high adhesiveness of CTCs should prevent their interactions with a variety of "chaperones", including monocytes.

4.2 Impact on other disciplines.
Nothing to Report

4.3 Impact on technology transfer.
Nothing to Report

4.3 Impact on society beyond science and technology.
Nothing to Report

5. Changes/problems

5.1 Changes in approach and reasons for change.

There are no significant changes in approach. Minor changes and additions include:

- Single-cell profiling (*Major Task 4, Subtasks 1and 2*). Since the single cells that are mechanically phenotyped have already assigned immunochemical phenotypes, we decided to collect additional sets of CTCs for single cell gene expression profiling and for multi-cell protein expression profiling, rather than transcriptionally profile only the post-AFM cells. The change increases the volume of information collected and available for the final model construction.

- Single-cell profiling (*Major Tasks 4, 5, 7*). We decided to add protein transcription profiling by flow cytometry/mass spectrometry CyTOF system to our analysis of TACCs

and cultured cells. This extremely effective technology became recently available in the UT Health BioAnalysis and Single Cell Core (BASiC). The change increases the volume of information collected and available for the final model construction.

- Cell culture models of CTCs and CTC-macrophage interactions (*Major Tasks 5 and 7*). We found that simulating fluid shear stress (FSS) that CTCs encounter in the bloodstream have a profound effect on the molecular and mechanical phenotypes of model CTCs. Therefore, we are including the FSS to our cell culture model experiments defining the role of EMT and CTC-macrophage interactions in metastatic potential of CTCs.

5.2 Actual or anticipated problems or delays.
None

5.3 Changes that had a significant impact on expenditures.
None

5.4 Significant changes in use or care of human subjects
None

5.5 Significant changes in use or care of vertebrate animals
None

5.6 Significant changes in use of biohazards and/or select agents.
None

6. Products

6.1 Publications, conference papers and presentations

6.1.1 Journal publications

- *Manuscript submitted (Cell Metabolism)* Acknowledgement of federal support: YES: Chia-Nung Hung,[1,2,9] Xi Tan,[1,9] Chun-Lin Lin,[1,9] Pawel A. Osmulski,[1] Liujie Wang,[1] Chih-Wei Chou,[1] Meizhen Chen,[1] Che-Kuang Lin,[1] Angela Chen,[1] Chiou-Miin Wang,[1] Nicholas Lucio,[1] Aaron M. Horning,[1] Kohzoh Mitsuya,[1] Josephine A. Taverna,[3] Zhijie Liu,[1] Kexin Xu,[1] Victor X. Jin,[1,4] Zhao Lai,[1,5] Dawn Garcia,[5] Qianben Wang,[6] Nameer Kirma,[1] Ian M. Thompson Jr.,[7] Maria E. Gaczynska,[1] Michael A. Liss,[8] Chun-Liang Chen,[1] Wei-Ting Chao,[2,*] and Tim H.-M. Huang[1,10,*] "Upregulation of Oxidative Phosphorylation for Cellular Adaptation of Hybrid Mesenchymal-Epithelial Trait In Circulating Prostate Tumor Cells"

6.1.2 Books or other non-periodical, one-time publications.
None

6.1.3 Other publications, conference papers and presentations.

- *Poster presented and Abstract published*: Acknowledgement of federal support: YES. Lin C-L, Xi T, Hung C-N, Osmulski PA, Chou C-W, Chen M, Wang C-M, Mitsuya K, Kirma N, Gaczynska ME, Chen C-L, Huang TH-M. Abstract 2766: Amplification-associated upregulation of genes involved in oxidative phosphorylation for disseminated prostate cancer cells. Cancer Res [Internet]. 2019 Jul 1;79(13 Supplement):2766 LP-2766. Available from: http://cancerres.aacrjournals.org/content/79/13_Supplement/2766.abstract

- *Other posters and presentations: see above in* **"3.4** Dissemination of the results to communities of interest". Acknowledgement of federal support: YES.

6.2 Website(s) or other Internet site(s)

Research program of the laboratory of Dr. Tim H. Huang, PI of the award is described and results are disseminated in the following page. The page contains the Research Program, list of publications and links to the PIs profile and laboratory personnel.

http://molecularmedicine.uthscsa.edu/FAC_Research.aspx?facID=133

6.3 Technologies or techniques
None

6.4 Inventions, patent applications, and/or licenses
None

6.5 Other Products
None

7. Participants

7.1 Individuals working on the project

Name	Tim H. Huang
Project Role	PI
Researcher Identifier (e.g. ORCID ID):	
Nearest person month worked:	0.96 cal. mo.
Contribution to Project:	Oversight and coordination of the project
Funding Support:	No Change

Name	Maria Gaczynska
Project Role	Co-Investigator
Researcher Identifier (e.g. ORCID ID):	0000-0002-9033-5706
Nearest person month worked:	3 cal. mo.
Contribution to Project:	Collection and analysis of immunofluorescence images of TACCs, design and oversight of co-culture experiments.
Funding Support:	No Change

Name	Pawel A.Osmulski
Project Role	Co-Investigator
Researcher Identifier (e.g. ORCID ID):	0000-0002-5359-9200
Nearest person month worked:	1.8 cal. mo.
Contribution to Project:	Collection and analysis of mechanical phenotypes of patient isolated and model CTCs, design of co-culture experiments.
Funding Support:	No Change

Name	Chun-Liang Chen
Project Role	Co-Investigator
Researcher Identifier (e.g. ORCID ID):	0000-0002-6774-9003
Nearest person month worked:	1.2 cal. mo.
Contribution to Project:	Collection of cells for single-cell gene expression analysis, single cell gene expression analysis of selected CTCs.
Funding Support:	No Change

Name	Michael Liss
Project Role	Co-Investigator
Researcher Identifier (e.g. ORCID ID):	0000-0001-6978-1026
Nearest person month worked:	.36 cal. mo.
Contribution to Project:	Coordination of patients' accrual, collection of clinical data.
Funding Support:	No Change

Name	Byeongyeob Choi
Project Role	Co-Investigator
Researcher Identifier (e.g. ORCID ID):	
Nearest person month worked:	.6 cal. mo.

Contribution to Project:	Processing of data for statistical analysis
Funding Support:	No Change

Name	Meizhen Chen
Project Role	Research Scientist
Researcher Identifier (e.g. ORCID ID):	
Nearest person month worked:	.6 cal. mo.
Contribution to Project:	Co-culture experiments with model CTCs and macrophages.
Funding Support:	No Change

Name	Chia-Nung Hung
Project Role	Research Scientist
Researcher Identifier (e.g. ORCID ID):	
Nearest person month worked:	3 cal. mo.
Contribution to Project:	CyTOF analysis of model CTCs and macrophages, collection of cells for single-cell gene expression analysis, single cell gene expression analysis of selected CTCs, model CTCs and model macrophages.
Funding Support:	No Change

Name	Yusheng Qian
Project Role	Graduate Student
Researcher Identifier (e.g. ORCID ID):	
Nearest person month worked:	6 cal. mo.
Contribution to Project:	Co-culture experiments with model CTCs and macrophages, collection and analysis of mechanical phenotypes of model CTCs.
Funding Support:	No Change

7.2 Changes in the active other support of PD/PI and key personnel
Nothing to report

7.3 Other organizations involved as partners
Nothing to report

8. Special Reporting Requirements
Nothing to report

9. Appendices

Upregulation of Oxidative Phosphorylation for Cellular Adaptation of Hybrid Mesenchymal-Epithelial Trait in Circulating Prostate Tumor Cells

Chia-Nung Hung,[1,2,9] Xi Tan,[1,9] Chun-Lin Lin,[1,9] Pawel A. Osmulski,[1] Liujie Wang,[1] Chih-Wei Chou,[1] Meizhen Chen,[1] Che-Kuang Lin,[1] Angela Chen,[1] Chiou-Miin Wang,[1] Nicholas Lucio,[1] Aaron M. Horning,[1] Kohzoh Mitsuya,[1] Josephine A. Taverna,[3] Zhijie Liu,[1] Kexin Xu,[1] Victor X. Jin,[1,4] Zhao Lai,[1,5] Dawn Garcia,[5] Qianben Wang,[6] Nameer Kirma,[1] Ian M. Thompson Jr.,[7] Maria E. Gaczynska,[1] Michael A. Liss,[8] Chun-Liang Chen,[1] Wei-Ting Chao,[2,*] and Tim H.-M. Huang[1,10,*]

[1]Department of Molecular Medicine, University of Texas Health Science Center at San Antonio, San Antonio, Texas, USA

[2]Department of Life Science, Tunghai University, Taichung, Taiwan

[3]Department of Medicine, University of Texas Health Science Center at San Antonio, San Antonio, Texas, USA

[4]Department of Epidemiology and Biostatistics, University of Texas Health Science Center at San Antonio, San Antonio, Texas, USA

[5]Greehey Children's Cancer Research Institute, San Antonio, Texas, USA

[6]Department of Pathology, Duke University, Durham, North Carolina, USA

[7]Texas Urology Group and CHRISTUS Santa Rosa Hospital – Medical Center, San Antonio, Texas, USA

[8]Department of Urology, University of Texas Health Science Center at San Antonio, San Antonio, Texas, USA

[9]These authors contributed equally

[10]Lead Contact

[*]Co-correspondence: wtchao@thu.edu.tw and huangt3@uthscsa.edu

SUMMARY

Circulating tumor cells (CTCs) shed from tumor sites have to withstand sudden changes of microenvironment in the bloodstream. Little is known about how CTCs metabolically adapt to vascular microenvironments. Here we show that the transcription of oxidative-phosphorylation (OXPHOS) genes is preferentially increased when compared to the expression levels of glycolysis genes in prostate CTCs. Menin, a multifaceted transcription factor, is found to upregulate transcriptional machineries of OXPHOS for mitochondrial respiratory functions. When tumor cells encounter glucose insufficiency, menin further acts as a metabolic sensor to boost the spare capacity of OXPHOS. This metabolic reprogramming supports ATP demands of tumor cells to elicit biophysical interchange between cellular mobility and adhesion. The hybrid mesenchymal-epithelial trait can be dynamically adapted by CTCs to enhance their survival in the circulation. Thus, the preferred usage of OXPHOS by these cells provides a window of therapeutic opportunity to target this metabolic pathway before CTC extravasation and metastasis.

INTRODUCTION

Tumor cells disseminated from primary or secondary sites invade surrounding tissues and migrate across endothelial layers of blood vessels for distant metastasis (Friedl and Alexander, 2011). These cells undergo multi-step processes of epithelial-mesenchymal transition (EMT) characterized by loss of cell-cell adhesion and apical-basal polarity and gains of mesenchymal traits for stromal invasion and intravasation into blood vessels (Chaffer and Weinberg, 2011; Friedl and Alexander, 2011). Distinct from primary tumor cells, circulating tumor cells (CTCs) have unique biophysical properties, enabling them to survive under metabolic stress in the circulation (Micalizzi et al., 2017; Thiele et al., 2017). Exhibiting high degrees of membrane flexibility and deformation, invasive CTCs can migrate through blood vessel wall into the organ parenchyma (Chaffer and Weinberg, 2011). Further supported by new microenvironments, viable tumor cells eventually start to proliferate to form metastatic colonies.

Emerging evidence implicates that CTCs may not go through complete EMT because these cells encounter drastic microenvironmental changes when entering the circulation (Nieto et al., 2016; Pastushenko et al., 2018). Although the majority of CTCs are subject to anoikis and apoptosis with a short half-life of <24 hr (Stott et al., 2010; Thiele et al., 2017), a small fraction of them can overcome the challenges in the harsh microenvironment. In addition to displaying mesenchymal characteristics for migration and invasion, it has been postulated that CTCs partially retain epithelial traits of cell-cell adhesion, allowing them to be tethered to chaperones as these cells travel in the circulation and then attach to vessel wall for extravasation (Sarioglu et al., 2015). To date, there is limited information available about selection of tumor cells to gain survival advantages in the vasculature. How intratumoral heterogeneity and clonal evolution of tumor cells are promoted by transcription reprogramming to overcome unfavorable vascular microenvironments remains to be determined.

In the present study, we used a systems approach to characterize CTCs isolated from prostate cancer patients. Differential genomic profiling identified amplified regions frequently

harbored overexpressed genes encoding metabolic functions in CTCs relative to primary tumor cells. Transcriptomic analysis further revealed preferential upregulation of oxidative-phosphorylation (OXPHOS) loci relative to other metabolic genes in CTCs. Integrative metabolic, proteomic, and biophysical profiling was conducted to assess altered phenotypes of prostate tumor cells *in vitro* and *in vivo*. It is known that primary tumor cells deploy redundant energy metabolisms, including the Warburg effect, in nutrient-rich microenvironments for active proliferation and growth (Vander Heiden et al., 2009). However, tumor cells may face a limited option for energy consumption in the blood circulation. We therefore explored a potential lack of redundant metabolic mechanisms in CTCs that could be an Achilles' heel for targeted therapies to hold off metastasis.

RESULTS

Preferential Upregulation of OXPHOS Gene Expression Occurs in CTCs

Increased exfoliation of neoplastic prostate epithelia due to weakening of cell-matrix contact can release tumor cells into the urinary tract (Botchkina et al., 2005). These urinary prostate cells (UPCs) sharing similar characteristics of primary tumor cells were used as surrogates for non-invasive cancer detection (Prensner et al., 2012). Invasive cells can also be shed from tumor sites into the blood circulation (Micalizzi et al., 2017). Therefore, prostate-specific exfoliated cells present in urine and blood of patients are valuable sources for comparative genomic analysis. We previously developed a technique to retrieve single exfoliated cells for which their cellular origin was confirmed with prostate-specific and stem-cell markers (Figure S1) (Pattabiraman and Weinberg, 2014; van der Toom et al., 2019). Initial genomic profiling of UPCs and CTCs (total 65 cells) was conducted in a patient who had bone metastasis (Patient #266, Figures 1A and 1B, and Table S1). Recurrent genomic alterations harboring well-known oncogenes (e.g., *MYC* on 8q) and tumor suppressor genes (e.g., *NKX3-1* on 8p*, PTEN* on 10q, *RB1* on 13q, and *CDH1* on 16q), respectively, were identified in these cells (Kumar et al., 2016;

Lapointe et al., 2007; Mendillo et al., 2012; Taylor et al., 2010). Hierarchical clustering analysis of genomic alterations categorized UPCs and CTCs into eight subpopulations (Figures 1C and 1D). Prior to therapies, three dominant subpopulations (#1, 2 and 3) were present in UPCs carrying common recurrent alterations. After the patient received therapies, the dominant subgroups were no longer present in UPCs or CTCs (Figures 1E and 1F). Instead, two new clones (#7 and 8) appeared, becoming the major CTC subpopulations (≥60%) without these recurrent alterations. Interestingly, these cells carried pre-existing and *de novo* alterations (e.g., 19p, 9p, 11p, and 20q) not originally present in the dominant subpopulations. These unique alterations in CTCs might contribute to the later development of castration resistance in this patient who showed rising PSA levels 10 months after the treatment (Figure 1B). To identify novel alterations, differential genomic analysis was further extended to 185 UPCs and 144 CTCs from a total of 17 patients (Table S1). A total of 261 genomic alterations were categorized into three groups: a) preferably amplified in UPCs; b) preferably amplified in CTCs; and c) amplified in both UPCs and CTCs (Figure 1G). Gene Ontology (GO) term enrichment analysis revealed that these genomic regions frequently harbored genes encoding various metabolic processes (e.g., Category c; Figure 1H), which have important adaptive functions for CTCs to survive in the blood circulation.

To further identify which pathways play a key role in metabolic adaptation, we conducted single-cell RNA-seq analysis of 136 CTCs isolated from 9 patients without prior therapies. Transcriptomic profiling of these CTCs showed striking overexpression of nuclear and mitochondrial genes encoding OXPHOS complexes I, II, III, IV and V, compared with other genes of five metabolic pathways, including glycolysis, glutamine, pentose phosphate pathway (PPP), fatty acid oxidation (FAO), and TCA cycle (Figure 2A). This overexpression could also be associated with nuclear OXPHOS genes localized on genomic regions that were frequently amplified or infrequently deleted in CTCs relative to UPCs (e.g., 5p12, 5p15.33, 9q34.2, 10q26.3, 16p13.3, 19p13.3, and 22q11.21; Figure S2). On average, there is a ~2-fold increase

in these genes relative to other metabolic genes in CTCs ($P < 0.001$; Figure 2B). In contrast, glycolysis genes appeared to be more frequently upregulated than OXPHOS genes in primary tumors known to use the Warburg effect for energy consumption (Figure S3) (Vander Heiden et al., 2009). These results suggest that CTCs initiate transcriptional reprogramming towards OXPHOS for a metabolic adaptation to vascular microenvironments.

Menin is a Transcriptional Regulator Involved in Mitochondrial Respiratory Functions

To determine how the transcriptional reprogramming is regulated, we searched transcription factors (TFs) encoded by loci that were co-expressed with metabolic gene modules in prostate cancer. Nuclear OXPHOS genes encoding different mitochondrial complexes are known to be co-regulated at the transcriptional level (Osman et al., 2018; van Waveren and Moraes, 2008). We therefore reasoned that a positive co-expression relationship implicates a cooperative regulatory role of a TF in these genes. mRNA expression data of 792 TF genes and OXPHOS and glycolysis genes from The Cancer Genome Atlas (TCGA) prostate dataset were used to perform co-expression analysis by the Pearson correlation coefficients (Figure 3A). Ten (1.3%) of TF-encoding genes - *MEN1, CREB3L4, SFPQ, URI1, CBX8, CRTC1, NRF1, GATA4, KLF15,* and *FOXN4* were positively correlated with the expression levels of OXPHOS genes, but not with those of glycolysis genes (Figure 3B). Among these positive loci, the top hit was *multiple endocrine neoplasia type 1* (*MEN1*) known to encode menin that participates in the development of castration-resistant prostate cancer (CRPC) (Malik et al., 2015).

To directly prove the regulatory role of menin in metabolic reprogramming, we selected a CRPC cell line PC3 as our experimental cell model because this cell line displayed overall higher expression levels of OXPHOS and other metabolic genes than those of two other less aggressive cell lines LNCaP and LNCaP-abl (Figure S4) (Higgins et al., 2009). shRNA knockdown of *MEN1* led to a decrease in mRNA levels of 14 selected genes participating in the assembly of mitochondrial complexes I (*NDUFS6* and *NDUFS7*), II (*SDHA* and *SDHB*), IV

(*SURF1*), and V (*ATP5F1D*) and in enzymatic reactions - vacuolar ATPase (*ATP6V0C*, *ATP6V1E1*), mitochondrial oxidation (*ECHS1* and *ECI1*), mitochondrial ribosomes (*MRPS30*), lipid peroxidation (*GPX4*), and intermembrane transport (*TIMM13* and *RHOT2*) (Figure 3C). Western immunoassay (WES) confirmed decreased protein levels in five of these loci using available antibodies (Figure 3D).

Metabolic profiling demonstrated a decline in oxygen consumption rate (OCR) of mitochondria for both basal and spare respiratory functions in *MEN1* knockdown relative to vehicle control cells ($P < 0.01$ and $P < 0.001$, respectively; Figure 3E). This reduction was accompanied with a 2-fold increase in non-mitochondrial respiration (NMR) likely mediated by NADPH oxidases to compensate OXPHOS deficiency (Chacko et al., 2014; Panday et al., 2014). However, the knockdown had no effect on glycolytic functions in PC3 cells, as determined by measuring profiles of extra cellular acidification rate (ECAR) (Figure 3F). We observed a slight increase in non-glycolytic acidification (NGA) in knockdown cells, contributed in part by other metabolic process like TCA cycle in response to OXPHOS deficiency ($P < 0.001$). With lowered OXPHOS activities, the production of ATP mostly switched to glycolysis for energy compensation in *MEN1* knockdown cells ($P < 0.001$; Figure 3G). Taken together, our finding identifies a previously uncharacterized role of menin in transcriptionally regulating OXPHOS in prostate tumor cells.

Menin-modulated Spare OXPHOS Capacity Facilitates Adaptation to Low Glucose

The above experiment was performed in a cell culture condition analogous to glucose-rich microenvironments in which tumor cells preferably break down glucose for ATP generation (Vander Heiden et al., 2009). However, CTCs traveling in the circulation faced a glucose-poor vascular microenvironment (glucose level ~5 mM) (Güemes et al., 2016). In addition, rapid mobilization of CTCs frequently hampers their glucose uptake in blood vessels. To investigate how restricted glucose availability influences menin-mediated OXPHOS reprogramming, we

treated vehicle control and *MEN1* knockdown PC3 cells at different glucose levels for 24 hr. Then, we measured OXPHOS and glycolysis functions with extracellular flux assays.

In both control and knockdown cells, NMR and basal OXPHOS functions were increased with decreasing glucose concentrations in the media (Figures 4A and 4B). Though less prominent, the enhanced basal functions were also seen in the second prostate cancer cell line LNCaP (Figure S5A). Interestingly, the spare respiratory capacity was first increased at 5.5 mM and then dropped at one tenth of the glucose level in control cells ($P < 0.001$). This reduced effect was even more dramatic when a miniscule amount of glucose was only available for *MEN1* knockdown cells.

Glycolytic functions were generally increased in glucose-starved PC3 cells after being re-challenged with glucose during ECAR measurement *in vitro* (Figures 4C and D) (Swerdlow, 2009). The overall production of ATP was dropped as a result of glucose starvation, although an increase in OXPHOS seemed to compensate the ATP loss in control cells (Figure 4E). Again, a similar observation was found in the second cell line LNCaP (Figures S5B and S5C). However, the ability to drive OXPHOS for the ATP production was diminished by dropping from 58% in control cells to 48% in *MEN1* knockdown cells. Interestingly, we noticed that the expression of *succinate dehydrogenase complex flavoprotein subunit A* and *B* (*SDHA* and *SDHB*) was also more reduced than other OXPHOS genes in knockdown cells (Figures 3C and 3D). These genes encode flavoprotein subunits that are critical elements of the mitochondrial complex II responsible not only for the electron transport chain and the TCA cycle, but also for the reserve respiratory capacity (Aspuria et al., 2014; Pfleger et al., 2015). While metformin is known to inhibit mitochondrial complex I (Pernicova and Korbonits, 2014), the antidiabetic agent also targets SDHA and SDHB leading to a greater attenuation of both basal and spare respiratory functions in circulating PC3 and LNCaP cells in an *in vitro* flow assay (Figure S6). Collectively, our findings suggest an additional role of menin in sensing glucose deficiency by upregulating the reserve respiratory capacity of the mitochondrial complex II.

Menin-regulated SDHA Enhances a Hybrid Mesenchymal-Epithelial Phenotype

Interestingly, SDHA was previously implicated as a mitochondrial tumor suppressor that prevents an EMT process (Aspuria et al., 2014). Therefore, we investigated whether increased SDHA can alter an EMT phenotype of PC3 cells using cytometry by time-of-flight (CyTOF) analysis of 8 mesenchymal (M) and 7 epithelial (E) protein markers. t-Distributed Stochastic Neighbor Embedding (t-SNE) profiling identified 25 subpopulations of PC3 cells after exposing to three different glucose concentrations - 11.0, 5.5, and 0.5 mM (Figures 5A and 5B). An overall increase in SDHA protein levels was observed in PC3 subpopulations exposed to low glucose conditions (#8-13 at 5.5 mM and #1-3, 5, and 10 at 0.5 mM; Figure 5C). When aligning these 25 subpopulations on the basis of increased SDHA amounts and individual subpopulation sizes, we were able to divide PC3 cells into three categories of E/M index: I) low expression of E and M markers; II) intermediate expression of E and M markers; and III) high expression of E and M markers (Figures 5D-F). Surprisingly, the majority of PC3 cells were assigned to Category III when these cells were exposed to 5.5 mM glucose equivalent to that of the normal blood (Figure 5G). Nevertheless, high E/M features appeared less prominent in cells exposed to 11 or 0.5 mM glucose. Therefore, prostate cancer cells displaying a hybrid E-M phenotype can be more adaptable to limited glucose availability in vascular microenvironments. The finding indicates that SDHA-associated spare respiratory capacity may push the maximal OXPHOS functions for cells to produce sufficient ATP needed to increase membranous plasticity under stressful conditions.

CTCs with a Hybrid Phenotype are Biophysically Adaptable to the Blood Circulation

Tumor cells with reversible plasticity have recently been shown to be more aggressive with high metastatic potential (Bidarra et al., 2016; Schliekelman et al., 2015). Aggressive CTCs need to be well adapted to withstand sheer forces in the blood circulation. Such mechanical adaptation

manifests, among others, with high deformability and elasticity (or softness) resembling mesenchymal rather than epithelial cells (Harouaka et al., 2013). Aggressive CTCs could also be highly adhesive, reminiscent of epithelial rather than mesenchymal cells (Huang et al., 2016; Osmulski et al., 2014). To assess mechanical phenotype of PC3 cells exposed to different glucose conditions, we used atomic force microscopy (AFM). AFM relies on a micrometer scale stylus nondestructively probing the surface of the cell to measure elasticity (kilopascals, kPa), deformation (nanometer, nm), and surface adhesion (picoNewton, pN) (Figures 6A and 6B). In general, PC3 cells (total 94) cultured under low glucose conditions, as compared to high glucose, displayed a trend of increased adhesiveness, deformability, and elasticity (Figure 6C). This biophysical analysis confirmed the CyTOF finding that PC3 cells converted to a hybrid phenotype when exposed to low glucose conditions. These cells exhibited not only high elasticity and deformability (a mesenchymal trait), but also elevated adhesiveness (an epithelial trait).

The AFM analysis was extended to 122 CTCs and 104 UPCs isolated from 27 prostate cancer patients. When principle component analysis (PCA) was used to stratify different biophysical features of these cells, we observed that cell adhesiveness showed the most striking difference among these exfoliated cells. CTCs appeared about five times more adhesive than UPCs (594 *versus* 107 pN) (Figure 6D). In contrast, one group of UPCs was ~50% softer (8.8 *versus* 16.6 kPa) and the other almost seven times stiffer than CTCs (126 *versus* 16.6 kPa). When CTCs alone were classified into three groups based on these biophysical parameters, we found that cells with increased elasticity, deformability, and adhesiveness frequently came from patients #40, 16, 42, 17 and 27 that had potential to develop CRPC after androgen-deprivation therapies (Figures 6E and 6F). Although high elasticity and deformability are known mesenchymal hallmarks of CTCs, the majority of CTCs usually retained epithelial adhesiveness. This result suggests that CTCs display hybrid traits that maintain high cell adhesiveness to enable survival-promoting clustering with other CTCs and chaperone cells, and attachment to

vessel walls for extravasation (Huang et al., 2016; Sarioglu et al., 2015). At the same time, the CTCs display mesenchymal properties for softness and deformability that may improve biophysical adaptation to shear force stress in the blood circulatory system.

DISSCUSSION

Although the normal function of cells depends on OXPHOS, tumor cells predominantly use glycolysis to produce energy even in the presence of abundant oxygen (Eidelman et al., 2017; Ippolito et al., 2016; Vander Heiden et al., 2009). This Warburg effect is thought to be the main metabolic pathway for ATP production in proliferating and metastatic tumor cells (Eidelman et al., 2017). However, emerging evidence implicates that invasive tumor cells still exploit OXPHOS in response to different microenvironmental cues for energy production (Ashton et al., 2018). In fact, cancer cells exhibit greater degrees of metabolic plasticity than normal cells to meet biosynthetic and energy requirements for growth and survival. There are approximately 300 nuclear and mitochondrial proteins participating in the assembly and control of OXPHOS machineries (Chacinska et al., 2009). To maintain energetic and biosynthetic homeostasis, OXPHOS is tightly regulated by post-translational and -transcriptional modifications and substrate feedback inhibition inside the cell (Koc and Koc, 2012; van Waveren and Moraes, 2008). Furthermore, promoter-binding sites are conserved among loci encoding similar mitochondrial functions, implicating co-regulation of these genes by common TFs at the transcription level (van Waveren and Moraes, 2008). Indeed, our co-expression correlation analysis and subsequent functional characterizations identify menin as a putative regulator of nuclear OXPHOS genes.

Whereas menin has a known suppressive role in tumors of the endocrine glands, its aberrant over-expression is frequently reported in other solid tumors (Dreijerink et al., 2017; Wu et al., 2017). The oncogenic function of menin is largely dependent on interaction with mixed lineage leukemia protein-1 or -2 (MLL1/2 or KMT2A/D), which is a SET domain-containing

histone methyltransferase that mediates trimethylation of histone H3 at lysine 4 (H3K4me3) for active transcription (Dreijerink et al., 2017; Wu et al., 2017). In addition to these epigenetic functions, more studies point to multifaceted actions of menin on transcriptional regulation of cell cycle, DNA repair, genomic instability, and stress response (Wu et al., 2010). Our present study further describes a previous unknown function of menin as a metabolic sensor. When entering the vasculature, tumor cells mostly encounter a sudden drop in glucose availability for glycolysis. Based on our current data, menin acts to upregulate the OXPHOS transcriptional program in response to the metabolic stress. Furthermore, menin regulates the transcription of *SDHA* and *SDHB*, which encode subunits of the mitochondrial complex II, for an increase in the spare respiratory capacity to meet energy demands and to promote cell survival (Pfleger et al., 2015).

Upregulated OXPHOS not only enhances survival capability of CTCs, but also supports energy requirements to increase their migratory and invasive capacity. While this increase in mesenchymal functions is required for metastasis, growing evidence suggests that these cells have the ability to partially revert back to an epithelial-cell state (Bidarra et al., 2016; Pastushenko et al., 2018; Schliekelman et al., 2015). Facing shear forces of blood flow, CTCs are capable of retaining an adhesion to form protective clusters or to attach to the vascular wall for extravasation (Chen et al., 2017; Sarioglu et al., 2015). Indeed, our CyTOF and AFM analyses confirmed that CTCs have a biphenotypic feature with both mesenchymal (i.e., more deformable and elastic) and epithelial (i.e., more adhesive) traits, compared with those of primary prostate tumor cells. Disseminated tumor cells retaining this epithelial trait can also increase their ability to tether to chaperones that support organelle trafficking of biomolecules for survival in the circulation. Tan and colleagues (Tan et al., 2015) demonstrated that mitochondria-depleted CTCs were able to recover mitochondria DNA from host cells through phagocytosis in a mouse model. This intercellular acquisition of the mitochondrial apparatus may greatly enhance survival of CTCs for extravascular invasion.

In summary, our present study identifies menin as a regulator of OXPHOS functions, which can be a crucial energy source for tumor cells to survive in the blood stream. The finding also supports the notion that a metabolic shift from the Warburg effect to OXPHOS is associated with biphenotypic traits of CTCs. Future work will define the mechanisms of OXPHOS and its by-products of mitochondrial biogenesis, such as reactive oxygen species (Ippolito et al., 2016), for the metastatic ability of these disseminated cells. The present finding, which is not evident through bulk analysis of primary and metastatic tumors, additionally provides a window of therapeutic opportunity to treat tumor cells in their vulnerable state in the circulation. To date, there are no biomarker-driven clinical studies specifically designed to explore the role of OXPHOS in prostate cancer or other malignancy. FDA-approved agents, like metformin, have the potential to target disseminated tumor cells in which OXPHOS is upregulated. In addition to receiving androgen-deprivation therapies, patients with early stage biochemical recurrence may be treated with metformin that has known minor side-effects and low toxicity (Rojas and Gomes, 2013). Expression profiling of OXPHOS genes in CTCs isolated from blood collected before, during, and after treatment can be used to assess patients' prognostic outcome.

SUPPLEMENTAL INFORMATION

Supplemental information includes six figures and four tables can be found with this article online.

ACKNOWLEDGMENTS

The authors are grateful for the contribution made from patients to this study. We also thank Mr. Joseph Liu, Drs. Guangcun Huang and Yao Wang, and the staff of the BioAnalytics and Single-Cell Core (BASiC) and the Next-Generation Sequencing Shared Resource at the University of Texas Health Science Center-San Antonio for providing their support of genomic and transcriptomic analyses. This work was supported by NIH grants U54CA217297,

P30CA054174, KL2TR001118 and 1S10OD021805-01, the CPRIT grant RP150600, the Department of Defense grant PC170821, the Ministry of Science and Technology of Taiwan MOST 106-2917-I-029-001, the San Antonio Cancer Foundation, the Max and Minnie Tomerlin Voelcker Fund, and the Alice P. McDermott Endowment. A.M.H. is a recipient of the predoctoral fellowship from the Cancer Biology Training Program T32CA148724. K.X. and Z.L. are CPRIT Scholars in Cancer Research (RR140072 and RR160017). Z.L. is also supported by V Foundation V2016-017 and DVP2019-018, Voelcker Fund Young Investigator award, and Susan G. Komen CCR award CCR17483391. J.A.T. is a KL2 scholar.

AUTHOR CONTRIBUTIONS

T.H.M.H., C.L.C. and M.A.L. conceived the work, designed the study, supervised the research and oversaw the project. C.L.C, C.L.L., C.N.H., P.A.O. and M.E.G. developed the protocols for experiments. C.L.L., X.T., C.N.H., P.A.O., M.E.G. and T.H.M.H. wrote and edited the manuscript. C.L.L. and X.T. performed statistical analyses. X.T. collected specimen and managed clinical information. C.L.C., X.T., C.N.H., C.W.C., C.K.L., M.C., L.W., A.C., C.M.W., N.L., J.L., A.M.H., K.M. and L.M. conducted experiments. P.A.O. and M.E.G. performed the AFM experiments and analyses. Z.L. and D.G. performed next-generation sequencing. I.M.T., J.A.T., Z.L., K.X., V.X.J., Q.W. W.T.C., N.K. and M.A.L. contributed scientific insight and edited the manuscript. I.M.T. and M.A.L. provided specimen.

DECLARATION OF INTERESTS

T.H.M.H. holds stock options and is on the Medical Advisory Board of LiSen Imprinting Diagnostics Wuxi Co., Ltd.

REFERENCES

Ashton, T.M., McKenna, W.G., Kunz-Schughart, L.A., and Higgins, G.S. (2018). Oxidative phosphorylation as an emerging target in cancer therapy. Clin. Cancer Res. *24*, 2482-2490.

Aspuria, P.-J.P., Lunt, S.Y., Väremo, L., Vergnes, L., Gozo, M., Beach, J.A., Salumbides, B., Reue, K., Wiedemeyer, W.R., Nielsen, J., et al. (2014). Succinate dehydrogenase inhibition leads to epithelial-mesenchymal transition and reprogrammed carbon metabolism. Cancer Metab. *2*, 21.

Bidarra, S.J., Oliveira, P., Rocha, S., Saraiva, D.P., Oliveira, C., and Barrias, C.C. (2016). A 3D in vitro model to explore the inter-conversion between epithelial and mesenchymal states during EMT and its reversion. Sci. Rep. *6*, 27072.

Botchkina, G.I., Kim, R.H., Botchkina, I.L., Kirshenbaum, A., Frischer, Z., and Adler, H.L. (2005). Noninvasive detection of prostate cancer by quantitative analysis of telomerase activity. Clin. Cancer Res. *11*, 3243-3249.

Chacinska, A., Koehler, C.M., Milenkovic, D., Lithgow, T., and Pfanner, N. (2009). Importing mitochondrial proteins: machineries and mechanisms. Cell *138*, 628-644.

Chacko, B.K., Kramer, P.A., Ravi, S., Benavides, G.A., Mitchell, T., Dranka, B.P., Ferrick, D., Singal, A.K., Ballinger, S.W., Bailey, S.M., et al. (2014). The Bioenergetic Health Index: a new concept in mitochondrial translational research. Clin Sci (Lond) *127*, 367-373.

Chaffer, C.L., and Weinberg, R.A. (2011). A perspective on cancer cell metastasis. Science *331*, 1559-1564.

Chen, C.-L., Mahalingam, D., Osmulski, P., Jadhav, R.R., Wang, C.-M., Leach, R.J., Chang, T.-C., Weitman, S.D., Kumar, A.P., Sun, L., et al. (2013). Single-cell analysis of circulating tumor cells identifies cumulative expression patterns of EMT-related genes in metastatic prostate cancer. Prostate *73*, 813-826.

Chen, H., Lau, M.C., Wong, M.T., Newell, E.W., Poidinger, M., and Chen, J. (2016). Cytofkit: A Bioconductor Package for an Integrated Mass Cytometry Data Analysis Pipeline. PLoS Comput Biol. *12*, e1005112.

Chen, L., Bode, A.M., and Dong, Z. (2017). Circulating tumor cells: moving biological insights into detection. Theranostics *7*, 2606-2619.

Dobin, A., Davis, C.A., Schlesinger, F., Drenkow, J., Zaleski, C., Jha, S., Batut, P., Chaisson, M., and Gingeras, T.R. (2013). STAR: ultrafast universal RNA-seq aligner. Bioinformatics *29*, 15-21.

Dreijerink, K.M.A., Groner, A.C., Vos, E.S.M., Font-Tello, A., Gu, L., Chi, D., Reyes, J., Cook, J., Lim, E., Lin, C.Y., et al. (2017). Enhancer-Mediated Oncogenic Function of the Menin Tumor Suppressor in Breast Cancer. Cell Rep *18*, 2359-2372.

Drost, J., Karthaus, W.R., Gao, D., Driehuis, E., Sawyers, C.L., Chen, Y., and Clevers, H. (2016). Organoid culture systems for prostate epithelial and cancer tissue. Nat. Protoc. *11*, 347-358.

Eidelman, E., Twum-Ampofo, J., Ansari, J., and Siddiqui, M.M. (2017). The metabolic phenotype of prostate cancer. Front. Oncol. *7*, 131.

Fabregat, A., Sidiropoulos, K., Viteri, G., Forner, O., Marin-Garcia, P., Arnau, V., D'Eustachio, P., Stein, L., and Hermjakob, H. (2017). Reactome pathway analysis: a high-performance in-memory approach. BMC bioinformatics *18*, 142.

Ferrick, D.A., Neilson, A., and Beeson, C. (2008). Advances in measuring cellular bioenergetics using extracellular flux. Drug Discov. Today *13*, 268-274.

Friedl, P., and Alexander, S. (2011). Cancer invasion and the microenvironment: plasticity and reciprocity. Cell *147*, 992-1009.

Gao, J., Aksoy, B.A., Dogrusoz, U., Dresdner, G., Gross, B., Sumer, S.O., Sun, Y., Jacobsen, A., Sinha, R., Larsson, E., et al. (2013). Integrative analysis of complex cancer genomics and clinical profiles using the cBioPortal. Sci. Signal. *6*, pl1.

Garvin, T., Aboukhalil, R., Kendall, J., Baslan, T., Atwal, G.S., Hicks, J., Wigler, M., and Schatz, M.C. (2015). Interactive analysis and assessment of single-cell copy-number variations. Nat. Methods. *12*, 1058-1060.

Han, H., Cho, J.W., Lee, S., Yun, A., Kim, H., Bae, D., Yang, S., Kim, C.Y., Lee, M., Kim, E., et al. (2018). TRRUST v2: an expanded reference database of human and mouse transcriptional regulatory interactions. Nucleic Acids Res. *46*, D380-D386.

Harouaka, R.A., Nisic, M., and Zheng, S.Y. (2013). Circulating tumor cell enrichment based on physical properties. J Lab Autom *18*, 455-468.

Higgins, L.H., Withers, H.G., Garbens, A., Love, H.D., Magnoni, L., Hayward, S.W., and Moyes, C.D. (2009). Hypoxia and the metabolic phenotype of prostate cancer cells. Biochim. Biophys. Acta *1787*, 1433-1443.

Hsu, Y.-T., Osmulski, P., Wang, Y., Huang, Y.-W., Liu, L., Ruan, J., Jin, V.X., Kirma, N.B., Gaczynska, M.E., and Huang, T.H.-M. (2016). EpCAM-regulated transcription exerts influences on nanomechanical properties of endometrial cancer cells that promote epithelial-to-mesenchymal transition. Cancer Res. *76*, 6171-6182.

Huang, G., Osmulski, P.A., Bouamar, H., Mahalingam, D., Lin, C.-L., Liss, M.A., Kumar, A.P., Chen, C.-L., Thompson, I.M., Sun, L.-Z., et al. (2016). TGF-β signal rewiring sustains epithelial-mesenchymal transition of circulating tumor cells in prostate cancer xenograft hosts. Oncotarget *7*, 77124-77137.

Ippolito, L., Marini, A., Cavallini, L., Morandi, A., Pietrovito, L., Pintus, G., Giannoni, E., Schrader, T., Puhr, M., Chiarugi, P., et al. (2016). Metabolic shift toward oxidative phosphorylation in docetaxel resistant prostate cancer cells. Oncotarget *7*, 61890-61904.

Iyer, S., Gaikwad, R.M., Subba Rao, V., Woodworth, C.D., and Sokolov, I. (2009). Atomic force microscopy detects differences in the surface brush of normal and cancerous cells. Nat. Nanotechnol. *4*, 389-393.

Kimball, A.K., Oko, L.M., Bullock, B.L., Nemenoff, R.A., van Dyk, L.F., and Clambey, E.T. (2018). A Beginner's Guide to Analyzing and Visualizing Mass Cytometry Data. Journal of immunology (Baltimore, Md. : 1950) *200*, 3-22.

Koc, E.C., and Koc, H. (2012). Regulation of mammalian mitochondrial translation by post-translational modifications. Biochim. Biophys. Acta *1819*, 1055-1066.

Kumar, A., Coleman, I., Morrissey, C., Zhang, X., True, L.D., Gulati, R., Etzioni, R., Bolouri, H., Montgomery, B., White, T., et al. (2016). Substantial interindividual and limited intraindividual genomic diversity among tumors from men with metastatic prostate cancer. Nat. Med. *22*, 369-378.

Langmead, B., and Salzberg, S.L. (2012). Fast gapped-read alignment with Bowtie 2. Nat. Methods. *9*, 357-359.

Lapointe, J., Li, C., Giacomini, C.P., Salari, K., Huang, S., Wang, P., Ferrari, M., Hernandez-Boussard, T., Brooks, J.D., and Pollack, J.R. (2007). Genomic profiling reveals alternative genetic pathways of prostate tumorigenesis. Cancer Res. *67*, 8504-8510.

Li, B., and Dewey, C.N. (2011). RSEM: accurate transcript quantification from RNA-Seq data with or without a reference genome. BMC Bioinformatics *12*, 323.

Li, H., Handsaker, B., Wysoker, A., Fennell, T., Ruan, J., Homer, N., Marth, G., Abecasis, G., Durbin, R., and Genome Project Data Processing, S. (2009). The Sequence Alignment/Map format and SAMtools. Bioinformatics *25*, 2078-2079.

Malek, A.M., Alper, S.L., and Izumo, S. (1999). Hemodynamic shear stress and its role in atherosclerosis. JAMA *282*, 2035-2042.

Malik, R., Khan, A.P., Asangani, I.A., Cieślik, M., Prensner, J.R., Wang, X., Iyer, M.K., Jiang, X., Borkin, D., Escara-Wilke, J., et al. (2015). Targeting the MLL complex in castration-resistant prostate cancer. Nat. Med. *21*, 344-52.

Mendillo, Marc L., Santagata, S., Koeva, M., Bell, George W., Hu, R., Tamimi, Rulla M., Fraenkel, E., Ince, Tan A., Whitesell, L., and Lindquist, S. (2012). HSF1 drives a transcriptional program distinct from heat shock to support highly malignant human cancers. Cell *150*, 549-562.

Mi, H., Poudel, S., Muruganujan, A., Casagrande, J.T., and Thomas, P.D. (2016). PANTHER version 10: expanded protein families and functions, and analysis tools. Nucleic acids research *44*, D336-342.

Micalizzi, D.S., Maheswaran, S., and Haber, D.A. (2017). A conduit to metastasis: circulating tumor cell biology. Genes Dev. *31*, 1827-1840.

Nieto, M.A., Huang, R.Y., Jackson, R.A., and Thiery, J.P. (2016). EMT: 2016. Cell *166*, 21-45.

Osman, N.M., Kitapci, T.H., Vlaho, S., Wunderlich, Z., and Nuzhdin, S.V. (2018). Inference of Transcription Factor Regulation Patterns Using Gene Expression Covariation in Natural Populations of Drosophila melanogaster. Biophysics (Oxf) *63*, 43-51.

Osmulski, P., Mahalingam, D., Gaczynska, M.E., Liu, J., Huang, S., Horning, A.M., Wang, C.-M., Thompson, I.M., Huang, T.H.M., and Chen, C.-L. (2014). Nanomechanical biomarkers of single circulating tumor cells for detection of castration resistant prostate cancer. Prostate *74*, 1297-1307.

Panday, A., Sahoo, M.K., Osorio, D., and Batra, S. (2014). NADPH oxidases: an overview from structure to innate immunity-associated pathologies. Cell Mol. Immunol. *12*, 5.

Pastushenko, I., Brisebarre, A., Sifrim, A., Fioramonti, M., Revenco, T., Boumahdi, S., Van Keymeulen, A., Brown, D., Moers, V., Lemaire, S., et al. (2018). Identification of the tumour transition states occurring during EMT. Nature *556*, 463-468.

Pattabiraman, D.R., and Weinberg, R.A. (2014). Tackling the cancer stem cells - what challenges do they pose? Nat. Rev. Drug Discov. *13*, 497-512.

Pernicova, I., and Korbonits, M. (2014). Metformin—mode of action and clinical implications for diabetes and cancer. Nat. Rev. Endocrinol. *10*, 143-56.

Pfleger, J., He, M., and Abdellatif, M. (2015). Mitochondrial complex II is a source of the reserve respiratory capacity that is regulated by metabolic sensors and promotes cell survival. Cell Death &Amp; Disease *6*, e1835.

Prensner, J.R., Rubin, M.A., Wei, J.T., and Chinnaiyan, A.M. (2012). Beyond PSA: the next generation of prostate cancer biomarkers. Sci. Transl. Med. *4*, 127rv123.

Rojas, L.B., and Gomes, M.B. (2013). Metformin: an old but still the best treatment for type 2 diabetes. Diabetol Metab Syndr *5*, 6.

Sarioglu, A.F., Aceto, N., Kojic, N., Donaldson, M.C., Zeinali, M., Hamza, B., Engstrom, A., Zhu, H., Sundaresan, T.K., Miyamoto, D.T., et al. (2015). A microfluidic device for label-free, physical capture of circulating tumor cell clusters. Nat. Methods *12*, 685-691.

Schliekelman, M.J., Taguchi, A., Zhu, J., Dai, X., Rodriguez, J., Celiktas, M., Zhang, Q., Chin, A., Wong, C.-H., Wang, H., et al. (2015). Molecular portraits of epithelial, mesenchymal, and hybrid States in lung adenocarcinoma and their relevance to survival. Cancer Res. *75*, 1789-1800.

Sokolov, I., Dokukin, M.E., and Guz, N.V. (2013). Method for quantitative measurements of the elastic modulus of biological cells in AFM indentation experiments. Methods *60*, 202-213.

Stott, S.L., Lee, R.J., Nagrath, S., Yu, M., Miyamoto, D.T., Ulkus, L., Inserra, E.J., Ulman, M., Springer, S., Nakamura, Z., et al. (2010). Isolation and characterization of circulating tumor cells from patients with localized and metastatic prostate cancer. Sci. Transl. Med. *2*, 25ra23.

Swerdlow, R.H. (2009). Mitochondrial Medicine and the Neurodegenerative Mitochondriopathies. Pharmaceuticals (Basel) *2*, 150-167.

Tan, An S., Baty, James W., Dong, L.-F., Bezawork-Geleta, A., Endaya, B., Goodwin, J., Bajzikova, M., Kovarova, J., Peterka, M., Yan, B., et al. (2015). Mitochondrial genome acquisition restores respiratory function and tumorigenic potential of cancer cells without mitochondrial DNA. Cell. Metab. *21*, 81-94.

Taylor, B.S., Schultz, N., Hieronymus, H., Gopalan, A., Xiao, Y.H., Carver, B.S., Arora, V.K., Kaushik, P., Cerami, E., Reva, B., et al. (2010). Integrative genomic profiling of human prostate cancer. Cancer Cell *18*, 11-22.

Thiele, J.A., Bethel, K., Králíčková, M., and Kuhn, P. (2017). Cell MetabolismCirculating tumor cells: fluid surrogates of solid tumors. Annu. Rev. Pathol. *12*, 419-447.

Van Der Maaten, L. (2015). Accelerating t-SNE using tree-based algorithms. J Mach Learn Res. *15*, 3221-3245.

Van Der Maaten, L., and Hinton, G. (2008). Visualizing data using t-SNE. J Mach Learn Res. *9*, 2579-2625.

van der Toom, E.E., Axelrod, H.D., de la Rosette, J.J., de Reijke, T.M., Pienta, K.J., and Valkenburg, K.C. (2019). Prostate-specific markers to identify rare prostate cancer cells in liquid biopsies. Nature Reviews Urology *16*, 7-22.

van Waveren, C., and Moraes, C.T. (2008). Transcriptional co-expression and co-regulation of genes coding for components of the oxidative phosphorylation system. BMC Genomics *9*, 18.

Vander Heiden, M.G., Cantley, L.C., and Thompson, C.B. (2009). Understanding the Warburg effect: the metabolic requirements of cell proliferation. Science *324*, 1029-1033.

Wu, G., Yuan, M., Shen, S., Ma, X., Fang, J., Zhu, L., Sun, L., Liu, Z., He, X., Huang, et al. (2017). Menin enhances c-Myc-mediated transcription to promote cancer progression. Nat. Commun. *8*, 15278.

Wu, T., Zhang, X., Huang, X., Yang, Y., and Hua, X. (2010). Regulation of cyclin B2 expression and cell cycle G2/m transition by menin. J. Biol. Chem. *285*, 18291-18300.

Xin, Y., Kim, J., Ni, M., Wei, Y., Okamoto, H., Lee, J., Adler, C., Cavino, K., Murphy, A.J., Yancopoulos, G.D., et al. (2016). Use of the Fluidigm C1 platform for RNA sequencing of single mouse pancreatic islet cells. Proc. Natl. Acad. Sci. USA *113*, 3293-3298.

FIGURE LEGENDS

Figure 1. Genomic Alterations of Urinary Prostate Cells (UPCs) and Circulating Tumor Cells (CTCs)

(A) Genomic profiles of the UPCs before (Pre-T UPCs) and during (T-UPCs) treatments, and CTCs during treatments (T-CTCs) of prostate cancer patient #266.

(B) Prostate-specific antigen (PSA) dynamics and clinical history of prostate cancer patient #266. The number of months reflects the relative time from the collection of the first urine sample used in the analysis. Timepoints of sample collections and critical clinical events are indicated with arrows.

(C) Sixty-five single cells on the amplification/deletion status at 32 dominant recurrent genomic alterations. The dendrogram shows single-cell clusters. The cells in close clusters were aggregated and assigned to 8 subgroups.

(D) Dominant recurrent genomic alterations in the eight clustering subgroups displayed as rectangles in the column under each subgroup.

(E) Proportion of cells clustered to the eight different subgroups in Pre-T UPCs, T-UPCs, and T-CTCs.

(F) Schematic model of clonal profiles of a prostate tumor before and after treatments.

(G) Focal amplifications in UPC and CTC groups. These genomic alterations are categorized into three categories (a to c) based on their unique or shared patterns in the two sample groups.

(H) Gene Ontology (GO) enrichment analysis of the corresponding genes mapped in the three categories of regions in (G).

See also Figures S1 and S2.

Figure 2. Single-cell Expression Profiles of Metabolic Genes in Circulating Tumor Cells (CTCs)

(A) Transcriptomic heat maps of genes associated with metabolic pathways, including glycolysis, pentose phosphate pathway (PPP), fatty acid oxidation (FAO), TCA cycle, glutamine, and five mitochondrial complexes (or OXPHOS).

(B) Violin plots displaying expression levels of genes associated with glycolysis, PPP, FAO, TCA cycle, glutamine, and OXPHOS in CTCs. ***P < 0.001 (Duncan's multiple range test).

See also Figure S3.

Figure 3. Identification of Menin as a Metabolic Regulator

(A) Flowchart of correlation analysis in glycolysis/OXPHOS expression and expression of transcription factors (TFs) based on The Cancer Genome Atlas (TCGA) cohort (*top panel*) and proportion of the five categories (*bottom panel*).

(B) Correlation scatter plots of glycolysis/OXPHOS expression and TF expression - *MEN1, CREB3L4, SFPQ, URI1, CBX8, CRTC1, NRF1, GATA4, KLF15,* and *FOXN4.*

(C-D) The expression levels of OXPHOS genes and proteins in vehicle control and *MEN1* knockdown PC3 prostate cancer cells.

(E) Oxygen consumption rate (OCR) curves and bar graphs of vehicle control and *MEN1* knockdown cells.

(F) Extracellular Acidification Rate (ECAR) curves and bar graphs of vehicle control and *MEN1* knockdown cells.

(G) ATP production rate of glycolysis and OXPHOS in vehicle control and *MEN1* knockdown cells.

Data are represented as mean ± SEM. **P < 0.01 and ***P < 0.001 (two-sided Student's t-tests).

See also Figure S4.

Figure 4. Menin-regulated Metabolic Profiles of Prostate Cancer Cells Cultured in Different Glucose Conditions

(A-B) Oxygen consumption rate (OCR) curves and bar graphs of vehicle control and *MEN1* knockdown cells cultured in 11.0, 5.5, and 0.5 mM glucose media.

(C-D) Extracellular Acidification Rate (ECAR) curves and bar graphs of vehicle control and *MEN1* knockdown cells cultured in 11.0, 5.5, and 0.5 mM glucose media.

(E) ATP production rate of glycolysis and OXPHOS in vehicle control and *MEN1* knockdown cells cultured in 11.0, 5.5, and 0.5 mM glucose media.

Data are represented as mean ± SEM. **P < 0.01, ***P < 0.001 (two-sided Student's t-tests).

See also Figures S5 and S6.

Figure 5. Mesenchymal-Epithelial Profiles of Prostate Cancer Cells Cultured in Different Glucose Conditions

(A-B) t-Distributed Stochastic Neighbor Embedding (t-SNE) projections of treatments and subpopulations of PC3 prostate cancer cells cultured 11.0, 5.5, and 0.5 mM glucose media.

(C) t-SNE scatter plots displaying expression profiles of SDHA and mesenchymal and epithelial markers in PC3 cell subpopulations.

(D) Subpopulations were aligned according to increased SDHA levels (violin plots) with size of each subpopulation in different glucose conditions shown below. Expression heat maps of mesenchymal and epithelial markers of each subpopulation were arranged accordingly. Cells were grouped into I, II and III categories of E/M index.

(E) Violin plots of mesenchymal (M) and epithelial (E) index in the three categories. ***P < 0.001 (Duncan's multiple range test).

(F) Scatter plots based on the expression of epithelial (E) and mesenchymal (M) markers in the three categories.

(G) Proportions of the three categories of PC3 cells cultured in 11.0, 5.5, and 0.5 mM glucose media.

Figure 6. Biophysical Profiles of Prostate Cancer Cells by Atomic Force Microscopy (AFM)

(A) *Left*: a light microscopy image of a CTC isolated from peripheral blood using a filter device. A black triangular cantilever is equipped with a tip perpendicularly pointing toward a viewer. Scale bar, 20 μm. *Right*: a 3D rendering of the AFM image collected in the height channel of the same cell presented to the left. Scale bar, 5 μm. A cartoon drawing of the cantilever and the tip is displayed in red (not to scale).

(B) Biophysical parameters calculated from AFM acquired force plots. Inserts illustrate distinct mechanical responses of cells to the indentation by the AFM tip during a probing cycle.

(C) Violin plots of three biophysical parameters – adhesion, deformation, and stiffness of PC3 prostate cancer cells exposed to 0.5, 5.5 and 11.0 mM for 24 hr. *P < 0.05, **P < 0.01, ***P < 0.001.

(D) Principal component analysis (PCA) separates populations of 122 CTCs and 104 UPCs.

(E) PCA allocates CTCs into three groups of distinct biophysical properties.

(F) Relative cell proportions in each CTC group as observed in (E) for castration-sensitive (CS) and castration-resistant (CR) prostate cancer patients after androgen-deprivation therapies.

STAR METHODS

CONTACT FOR REAGENT AND RESOURCE SHARING

Further information and requests for resources and reagents should be directed to and will be fulfilled by the Lead Contact, Tim H.-M. Huang (huangt3@uthscsa.edu).

EXPERIMENTAL MODEL AND SUBJECT DETAILS

Human Subjects

The post-digital rectal examination (post-DRE) or early morning void urine and/or blood samples of prostate needle biopsy patients and/or prostate cancer patients were collected following the IRB protocols at the University of Texas Health Science Center at San Antonio and the Audie L. Murphy Memorial VA Hospital. Informed consent was obtained from all subjects. All patients in this study were male in gender. Detailed clinicopathological information on individual patients in this study are provided in Table S1.

Cell Lines

PC3 prostate cancer cells (male, 62 years old, prostate adenocarcinoma derived from metastatic site) were cultured in RPMI-1640 medium supplemented with 10% fetal bovine serum and 100 U/mL penicillin/streptomycin. LNCaP prostate cancer cells (male, 50 years old, prostate carcinoma derived from metastatic site) were cultured in RPMI-1640 medium supplemented with 10% fetal bovine serum and 100 U/mL penicillin/streptomycin. LNCaP-abl prostate cancer cells were cultured in RPMI-1640 phenol-red free medium supplemented with 10% charcoal stripped fetal bovine serum and 100 U/mL penicillin/streptomycin. The authenticity of these cell lines was performed by the STR Testing Service of the American Type Culture Collection.

METHOD DETAILS

Urine and Blood Sample Collection

Void urine was collected in urine cup (Starplex Scientific) and blood was collected in EDTA-coated tubes (Becton, Dickinson and Company) for subsequent analysis after patients' enrollment with informed consents.

DEPArray

Urinary cells were fixed with added 1% paraformaldehyde in urine samples at room temperature (RT) for 15 min. Cells were centrifuged at 1,600 g for 5 min. After removing supernatants, cell pellets were suspended with 1 mL 1X PBS and centrifuged at 1,600 g for 20 sec. Cells were permeated with 1 mL PBS+5% FBS+0.2% Tween 20 at RT for 10 min and centrifuged at 1,600 g for 20 sec. Cells were labeled with polyclonal rabbit α-PSA (1:100, Dako, #A0562) and α-hPSMA/FOLH1-APC (1:10, R&D system, #FAB4234A) in 100 µL PBS+5%FBS+0.2% Tween 20 on ice for 15 min with light proof. Cells were centrifuged for 20 sec and washed twice with 1 mL PBS+5% FBS+0.2% Tween 20 to remove remnant antibodies. PSA was visualized with anti-rabbit IgG-Cy3 (1:500, Jackson ImmunoResearch Lab, #111-166-003) in 100 µL PBS+5% FBS+0.2% Tween 20+0.5 µg/mL DAPI (1:100 dilution) at RT for 15 min. The cells were centrifuged for 20 sec and washed twice with 500 µL SB115 buffer to remove the secondary antibody. The cells were resuspended in 20 µL SB115 buffer and degassed using sonication for 15 min before loaded onto A300K cartridge (Silicon Biosystems). For cell image analysis, the DEArray system was used to trap individual cells in "electric cages" for counting. Single-cell fluorescence intensity for PSA and PSMA was subject to DEPArray analysis with the integrated software according to the protocol from the Silicon Biosystems.

Isolation of Urinary Prostate Cells (UPCs)

Exfoliated cellular components from void urine were centrifuged at 700 g for 5 min and collected by removal of supernatant. The cellular pellets were washed with cold 1 mL of 1X PBS and recollected by centrifugation twice. The pellets were suspended and labeled with α-PSA (1:100, Dako, #A0562) and α-hPSMA/FOLH1-APC (1:10, R&D system, #FAB4234A) for 15 min on ice and followed by secondary antibody incubation of anti-rabbit IgG-Cy3, (1:500, Jackson ImmunoResearch Lab, #111-166-003) in 200 µL DMEM+5%FBS+P/S (2x) and 0.5 µg/mL DAPI on ice for 15 min. To isolate single cells, a micromanipulator was applied to manually retrieve a PSA/PSMA-positive cell with a micropipette tip in an inverted EVOS FL microscope (Life Technologies) using an established protocol (Chen et al., 2013).

Isolation and Characterization of Circulating Tumor Cells (CTCs)

CTCs were isolated from 8-16 mL of patient blood following a previous protocol with modifications (Drost et al., 2016). After Ficoll cushion centrifugation, the interphase portion of the blood was collected. The CD45-positive cells were depleted using MojoSort™ Human CD45 Nanobeads (BioLegend, #480030), followed by second depletion when CD45-positive cells remained. The remaining cells were centrifuged and cultured in 0.5 mL PRIME-XV tumorsphere medium (Irvine Scientific, #91130) for CTC enrichment. CTCs were expanded and grown as tumor spheres for 1 to 2 weeks aired with CO_2 at 37^{o}C. Residual CD45-positive cells might additionally be removed from cell cultures by nanobead depletion before immunofluorescence analysis. The cells were fixed with 4% paraformaldehyde for 20 min and penetrated with 0.2% Triton-X/5% FBS/PBS. Two washes of PBS were followed. The cells labeled with anti-CD133, -CD44, -ALDH1A, -OCT4, -NANOG, -CD45, -EpCAM (1:200, Abcam), and -PSA (Cell Signaling Technology) conjugated with fluorescence and DAPI in DMEM/5%FBS/1%P/S were evaluated and documented using confocal microscope Zeiss 510 NLO (Zeiss).

Single-cell Genomic Sequencing

Single UPCs and CTCs were subject to whole genome amplification (WGA) using REPLI-g Single Cell Kit (Qiagen, #150345). In order to avoid contamination from the environment, WGA procedure was conducted in a UV-treated laminar-flow cabinet in a dedicated clean room with controlled air pressure. WGA products were used for PCR amplification using primers for reference genes, and samples with positive amplification were further prepared for sequencing with purification by Agencourt AMPure XP beads (Beckman Coulter, #A63881) and quantification using Qubit fluorometer (Invitrogen, #Q32866). The whole genome amplified DNA (~250 ng) was used for DNA-seq library preparation with KAPA HyperPlus Library Preparation Kit (KAPA Biosystems, #KK8514). The clustering of the index-coded samples was performed on a cBot cluster generation system. Sequencing run was carried out on the Illumina HiSeq 3000 platform following standard protocols. FASTQ files for each sample were generated from the output via demultiplexing with the bcl2fastq2 conversion software (v2.16). Paired-end FASTQ files were aligned to the human reference genome GRCh37 using Bowtie 2 alignment software (Langmead and Salzberg, 2012). SAMtools (Li et al., 2009) was used to convert compressed SAM files to BAM file, which were then sorted and indexed. PCR duplicates were removed by SAMtools. Sequence reads with low mapping quality (MAPQ < 35) were excluded from the downstream analysis.

Genomic Alteration Analysis

The open source software Ginkgo was first used to analyze genomic alteration of single cells from BAM files (Garvin et al., 2015). Mapping reads were first binned into variable-length intervals across the genome at bin sizes 250- and 100-kb. After quality control and biases correction, the final normalized and segmented bin counts, with value 1 as the diploid standard,

were used for downstream analyses. We considered count values ≥1.15 as amplification and ≤0.85 as deletion.

Recurrent alterations were identified as a series of consecutive bins where amplification or deletion were observed in ≥25% of the cells. Hierarchical clustering was performed on the binary format of recurrent alterations, where 1 was given when ≥80% of the bins in the regions were amplified/deleted, and otherwise 0 was given. Distances between each cell were calculated using the R function dist, and then the cells were clustered with the Ward method. After clustering, the number of subpopulations was determined using the R function cutree. Dominant alterations in each subgroup were defined as ≥70% of cells amplified/deleted in each subgroup.

Focal amplifications were identified in each single cell considering their similarity in a focal region (~5 Mb) and dissimilarity to neighbor bins, where 50 or less adjacent bins continually displayed amplification while showing relatively large differences from the neighboring bins. Recurrent focal amplification regions in a patient were defined based on cumulative occurrences of amplification of at least 3 cells. The recurrent focal amplification regions of all cells were the union of the regions of individual patients. Mann-Whitney U tests were used to test the significance of bin counts of each region between UPCs and CTCs to categorize regions into groups a, b and c. Gene Ontology (GO) term enrichment analysis was performed on the genes within the regions of categories a, b and c separately using the Gene Ontology Consortium (http://geneontology.org/) based on GO databases in PANTHER (Fabregat et al., 2017; Mi et al., 2016)

Single-cell RNA-seq

Single-cell cDNA libraries of CTCs were prepared and generated with Fluidigm C1 (Xin et al., 2016). cDNA sequencing was performed on Illumina HiSeq 3000, and the output paired-end

FASTQ files were aligned to the GRCh38 reference genome using STAR alignment software (Dobin et al., 2013). RSEM was applied to quantify gene expression levels (Li and Dewey, 2011), and Fragments Per Kilobase of transcript per Million (FPKM) mapped reads were calculated.

In silico Analysis of Prostate Tumor Cohort

Transcription factor (TF) encoding genes were downloaded from the TRRUST database (Han et al., 2018). The copy number and RNA-seq data of The Cancer Genome Atlas (TCGA) cohort were downloaded from the cBioPortal for Cancer Genomics (Gao et al., 2013). The expression of 45 glycolysis, 108 OXPHOS genes and 792 TF encoding genes were then extracted. After removing genes with low expression, average glycolysis and OXPHOS expression were calculated. The correlation analysis was conducted on the expression of every TF encoding gene and the average glycolysis/OXPHOS expression. For the survival analysis of Figure S2, the discrete copy number data based on GISTIC algorithms were used. Groups with copy-number gains were tumors with the sum of total copy-numbers of the 14 OXPHOS genes ≥0, while no-change group equal to 0. Expression levels were normalized to a reference population first, and the sum of expression levels of the 14 OXPHOS genes was used to group the tumors of the TCGA cohort into High (≥10), Intermediate (-10 to <10), and Low groups (< -10).

Protein and mRNA Analyses

Cells were infected by lentivirus with sh*MEN1* and vehicle plasmid. The 2nd Generation Packaging Mix (abm) was used for sh*MEN1* Lentivirus infection preparation following manufacturer's instruction. Infected cells were selected with 4 ng/μl puromycin for 5 days and then protein lysates and total RNAs were harvested after 9 days of infection. Protein lysates were then analyzed in 12-230 kDa Wes Separation Module of quantitative capillary Western

immunoassay system (ProteinSimple) with anti-Rabbit or anti-mouse detection module (ProteinSimple) to detect protein levels of ATP5F1A, ATP5F1D, GPX4, Menin, SDHA, SDHB, and GAPDH. Dual antibodies (target antibody and GAPDH) were applied in the same sample of each capillary Western blotting to increase the accuracy of normalization by GAPDH. Total RNA (500 ng/μL) of each sample was converted to cDNA with High-Capacity cDNA Reverse Transcription Kit (Applied Biosystems) following manufacturer's instruction. Quantitative PCR was performed with Power SYBR™ Green PCR Master Mix (Applied Biosystems) in the Mx3005P QPCR System (Agilent). Fold changes of all OXPHOS genes expression levels were calculated using comparative ΔΔCt method.

Measurement of Cellular OCR and ECAR

Cells (~1.5 x 10^4), respectively, were seeded on poly-L-lysine coated 96-well seahorse plate and treated with different glucose concentrations (11.0, 5.5, 0.5 and 0 mM) for 24 hr. Measurement of extracellular flux of cellular bioenergetics was determined by a Seahorse XFe96 Extracellular Flux Analyzer (Ferrick et al., 2008). OCR and ECAR were normalized based on cell number (1000 cells) of each well counted by Cytation 1 (BioTek).

Single-cell Proteomics Analysis by Mass Cytometry (CyTOF)

Cells were treated with different glucose concentrations (11 mM, 5.5 mM, and 0.5 mM) for 24 hr before incubated with antibodies. Antibodies were either conjugated in-house according to the manufacturer's instructions (Fluidigm, South San Francisco, CA) or purchased in conjugated forms from the supplier (Fluidigm). The cells were detached into single cell suspension and stained with cisplatin (Fluidigm) to label dead cells. After fixation and permeabilization, the intracellular staining with metal-conjugated antibodies was performed. Cells were then labeled with an iridium-containing DNA intercalator ($^{191}Ir^+$, $^{193}Ir^+$) to identify cell events before analysis on

a Helios mass cytometer (Fluidigm). Signals were bead-normalized using EQ Four Element Calibration Beads (Fluidigm).

Signals of samples were normalized using CyTOF software (Version 6.7.1014, Fluidigm), followed by signal cleanup and live/dead cells filtering using Cytobank (https://www.cytobank.org/, Cytobank Inc.). Gated FCS file was exported for further analysis using PhenoGraph algorithm based Cytofkit (Chen et al., 2016; Kimball et al., 2018), which was available from the Bioconductor website (https://bioconductor.org/packages/cytofkit/) and ran program in R. CyTOF data were displayed using *t*-SNE (Van Der Maaten, 2015; Van Der Maaten and Hinton, 2008) and plotted on a continuum of expression with phenotypically related cells clustered together.

Atomic Force Microscopy (AFM)

Cells were seeded on poly-L-lysine plates and treated with different glucose concentrations (11.0, 5.5, and 0.5 mM) for 24 hr. CTCs were isolated from patients' blood with ScreenCell filters and imaged directly on the filter after staining for EpCAM and N-cadherin following the established protocols (Huang et al., 2016; Osmulski et al., 2014). UPCs captured on glass slides coated with 0.1% polyethylenimine (Sigma-Aldrich) were immune stained for EpCAM and CD44 after 30 min incubation in DMEM. PC3 cells, CTCs and UPCs were scanned with a Catalyst Atomic Force Microscope (Bruker) mounted on a Nikon Ti inverted epifluorescent microscope. Nanomechanical parameters of cells were collected in the Quantitative Nanomechanical Mapping (PF-QNM) mode of the AFM. Before AFM imaging, optical images were recorded for each cell. SCANASYST-AIR (Bruker) probes were used for imaging after their spring constant was determined with the thermal tuning. Cell boundaries were located with peak force error (PFE) AFM images and further verified with height images. Nanomechanical parameters of cells were captured in three separate PF-QNM channels: elasticity (Young's modulus), deformation and adhesion. Analysis of these parameters was performed with

NanoScope Analysis software v.1.7 (Bruker) using the retrace images (Hsu et al., 2016). Force curves were fitted to the Sneddon model, which additionally included adhesion forces and followed the rules proposed by Sokolov (Iyer et al., 2009; Sokolov et al., 2013). Mode values of the mechanical parameters for individual cells were calculated from the corresponding distribution histograms.

In vitro Proliferation Assay

Cells ($6x10^3$) were seeded in 96-well plate and treated with a range of metformin doses over the course of 48 hr. Cell confluence images were acquired every 3 hr over a 48 hr timeframe with IncuCyte ZOOM (Essen BioScience) to generate proliferation curves. Data were normalized to controls, and values for the half maximal inhibitory concentration were calculated using Prism V8.0 (GraphPad software).

In vitro Flow Assay and Cell Viability

Cells (~10^6) with or without 4 mM metformin treatment were trypsinized, resuspended in 5.5 mM glucose (10 mL), loaded in the ibidi Pump System connected with 0.6 mm µ–Slide and circulated for 1 hr. Pump system was set up at 16.65 ml/min flow rate to generate 7 dyn/cm^2 shear stress to simulate microvascular wall shear stress (Malek et al., 1999). After 1 hr circulation, cells were harvested for cell viability test and measurement of extracellular flux of cellular bioenergetics. Cell viability was determined by CellTiter-Glo Luminescent Cell Viability Assay Kit (Promega, #G7571) according to manufacturer's instruction. The luminescence of each sample was measured in Luminoskan Ascent Microplate Luminometer.

Statistical Analysis

The Kaplan-Meier curves among sample groups were constructed by R package *survival* and the G-rho family of tests was implemented. Duncan's multiple range test was implemented when comparing multiple groups. Principle component analysis on the biophysical phenotypes of cells was performed using Origin software (OriginLab) and confirmed by Statistica (TIBCO).

DATA AND SOFTWARE AVAILABILITY

The raw DNA sequencing data have been deposited in NCBI Sequence Read Archive under accession SRP123720 and raw RNA-seq data in GEO under accession GSE115501.

Supplemental Information

Table S1. Clinicopathological information of patients. Related to Figure 1

Table S2. DNA sequencing statistics. Related to STAR Methods

Table S3. RNA sequencing statistics. Related to STAR Methods

Table S4. Primer sequence of quantitative RT-PCR. Related to Figures 3

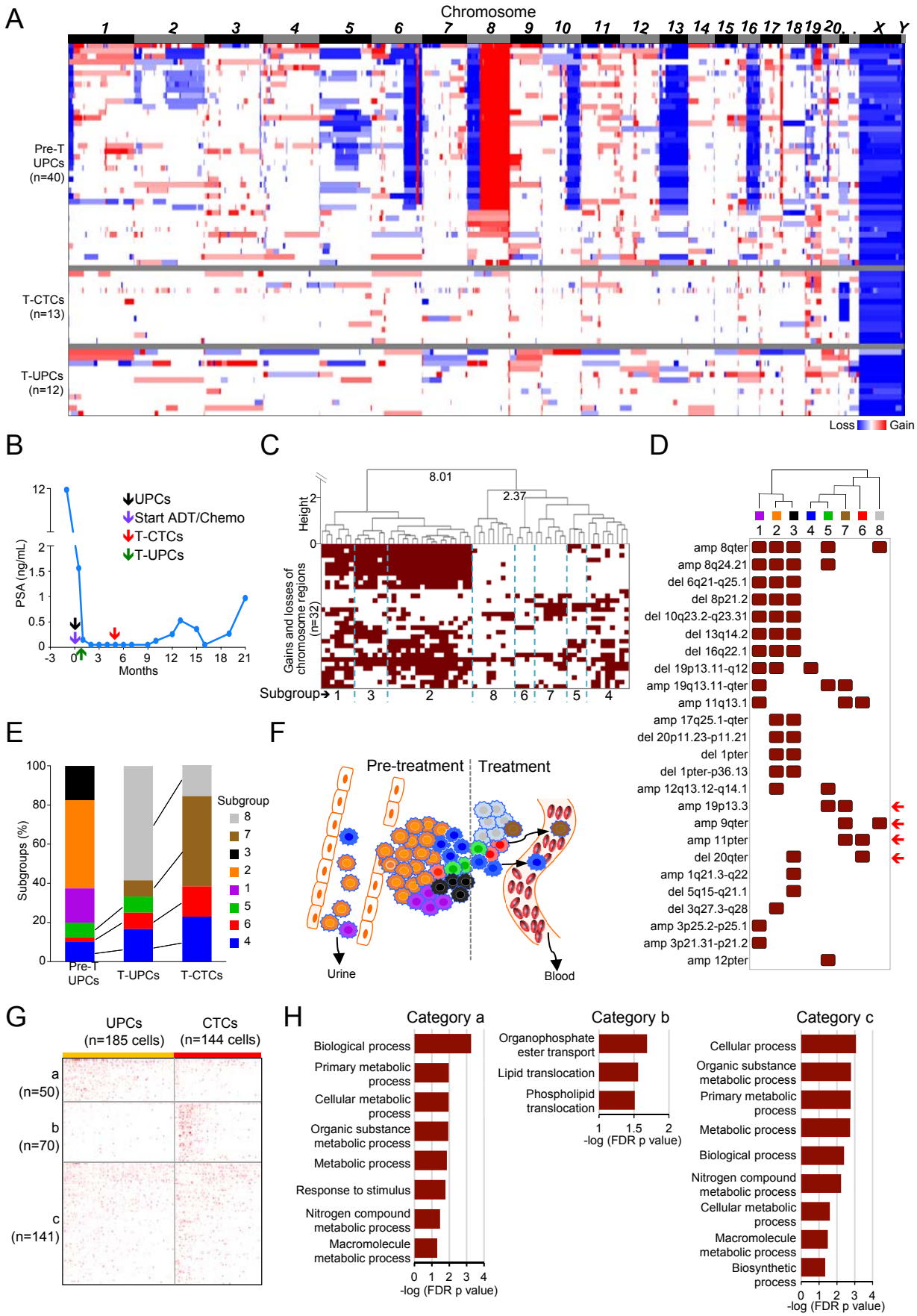
A
Chromosome
1 2 3 4 5 6 7 8 9 10 11 12 13 14 15 16 17 18 19 20 X Y
Pre-T UPCs (n=40)
T-CTCs (n=13)
T-UPCs (n=12)
Loss Gain
B
PSA (ng/mL)
Months
UPCs
Start ADT/Chemo
T-CTCs
T-UPCs
C
8.01
2.37
Height
Gains and losses of chromosome regions (n=32)
Subgroup 1 3 2 8 6 7 5 4
D
1 2 3 4 5 7 6 8
amp 8qter
amp 8q24.21
del 6q21-q25.1
del 8p21.2
del 10q23.2-q23.31
del 13q14.2
del 16q22.1
del 19p13.11-q12
amp 19q13.11-qter
amp 11q13.1
amp 17q25.1-qter
del 20p11.23-p11.21
del 1pter
del 1pter-p36.13
amp 12q13.12-q14.1
amp 19p13.3
amp 9qter
amp 11pter
del 20qter
amp 1q21.3-q22
del 5q15-q21.1
del 3q27.3-q28
amp 3p25.2-p25.1
amp 3p21.31-p21.2
amp 12pter
E
Subgroups (%)
Subgroup 8 7 3 2 1 5 6 4
Pre-UPCs
T-UPCs
T-CTCs
F
Pre-treatment
Treatment
Urine
Blood
G
UPCs (n=185 cells)
CTCs (n=144 cells)
a (n=50)
b (n=70)
c (n=141)
H
Category a
Biological process
Primary metabolic process
Cellular metabolic process
Organic substance metabolic process
Metabolic process
Response to stimulus
Nitrogen compound metabolic process
Macromolecule metabolic process
-log (FDR p value)
Category b
Organophosphate ester transport
Lipid translocation
Phospholipid translocation
-log (FDR p value)
Category c
Cellular process
Organic substance metabolic process
Primary metabolic process
Metabolic process
Biological process
Nitrogen compound metabolic process
Cellular metabolic process
Macromolecule metabolic process
Biosynthetic process
-log (FDR p value)

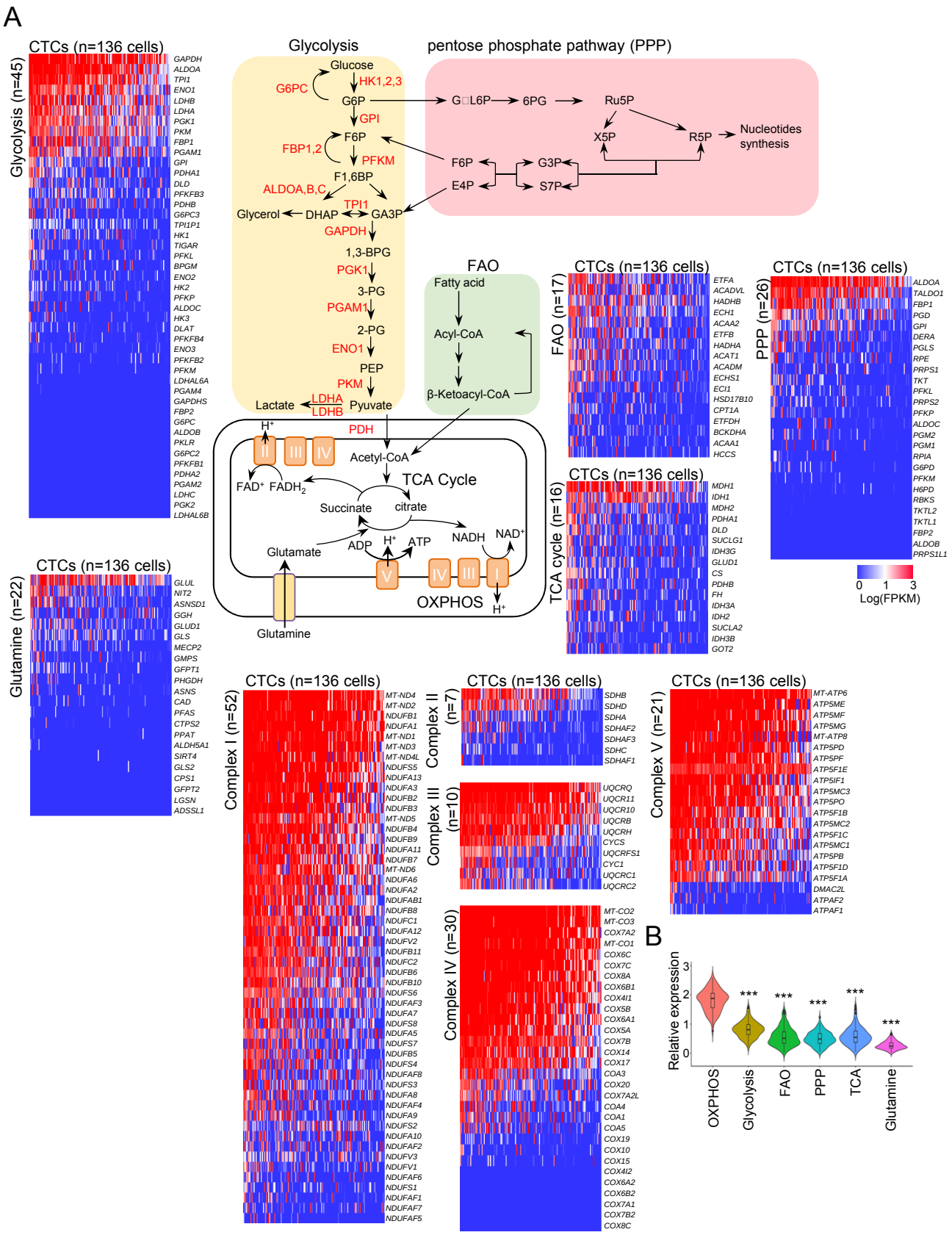
A
CTCs (n=136 cells)
Glycolysis (n=45)
GAPDH
ALDOA
TPI1
ENO1
LDHB
LDHA
PGK1
PKM
FBP1
PGAM1
GPI
PDHA1
DLD
PFKFB3
PDHB
G6PC3
TPI1P1
HK1
TIGAR
PFKL
BPGM
ENO2
HK2
PFKP
ALDOC
HK3
DLAT
PFKFB4
ENO3
PFKFB2
PFKM
LDHAL6A
PGAM4
GAPDHS
FBP2
G6PC
ALDOB
PKLR
G6PC2
PFKFB1
PDHA2
PGAM2
LDHC
PGK2
LDHAL6B
Glycolysis
Glucose
G6PC
HK1,2,3
G6P
GPI
F6P
FBP1,2
PFKM
F1,6BP
ALDOA,B,C
TPI1
Glycerol
DHAP
GA3P
GAPDH
1,3-BPG
PGK1
3-PG
PGAM1
2-PG
ENO1
PEP
PKM
Lactate
LDHA
LDHB
Pyuvate
pentose phosphate pathway (PPP)
G6P
6PG
Ru5P
X5P
R5P
Nucleotides synthesis
F6P
G3P
E4P
S7P
FAO
Fatty acid
Acyl-CoA
β-Ketoacyl-CoA
PDH
Acetyl-CoA
TCA Cycle
Succinate
citrate
FAD+
FADH2
NADH
NAD+
ADP
ATP
H+
Glutamate
Glutamine
OXPHOS
CTCs (n=136 cells)
FAO (n=17)
ETFA
ACADVL
HADHB
ECH1
ACAA2
ETFB
HADHA
ACAT1
ACADM
ECHS1
ECI1
HSD17B10
CPT1A
ETFDH
BCKDHA
ACAA1
HCCS
CTCs (n=136 cells)
PPP (n=26)
ALDOA
TALDO1
FBP1
PGD
GPI
DERA
PGLS
RPE
PRPS1
TKT
PFKL
PRPS2
PFKP
ALDOC
PGM2
PGM1
RPIA
G6PD
PFKM
H6PD
RBKS
TKTL2
TKTL1
FBP2
ALDOB
PRPS1L1
0
1
3
Log(FPKM)
CTCs (n=136 cells)
TCA cycle (n=16)
MDH1
IDH1
MDH2
PDHA1
DLD
SUCLG1
IDH3G
GLUD1
CS
PDHB
FH
IDH3A
IDH2
SUCLA2
IDH3B
GOT2
CTCs (n=136 cells)
Glutamine (n=22)
GLUL
NIT2
ASNSD1
GGH
GLUD1
GLS
MECP2
GMPS
GFPT1
PHGDH
ASNS
CAD
PFAS
CTPS2
PPAT
ALDH5A1
SIRT4
GLS2
CPS1
GFPT2
LGSN
ADSSL1
CTCs (n=136 cells)
Complex I (n=52)
MT-ND4
MT-ND2
NDUFB1
NDUFA1
MT-ND1
MT-ND3
MT-ND4L
NDUFS5
NDUFA13
NDUFA3
NDUFB2
NDUFB3
MT-ND5
NDUFB4
NDUFB9
NDUFA11
NDUFB7
MT-ND6
NDUFA6
NDUFA2
NDUFAB1
NDUFB8
NDUFC1
NDUFA12
NDUFV2
NDUFB11
NDUFC2
NDUFB6
NDUFB10
NDUFS6
NDUFAF3
NDUFA7
NDUFS8
NDUFA5
NDUFS7
NDUFB5
NDUFS4
NDUFAF8
NDUFS3
NDUFA8
NDUFAF4
NDUFA9
NDUFS2
NDUFA10
NDUFAF2
NDUFV3
NDUFV1
NDUFAF6
NDUFS1
NDUFAF1
NDUFAF7
NDUFAF5
CTCs (n=136 cells)
Complex II (n=7)
SDHB
SDHD
SDHA
SDHAF2
SDHAF3
SDHC
SDHAF1
CTCs (n=136 cells)
Complex III (n=10)
UQCRQ
UQCR11
UQCR10
UQCRB
UQCRH
CYCS
UQCRFS1
CYC1
UQCRC1
UQCRC2
CTCs (n=136 cells)
Complex IV (n=30)
MT-CO2
MT-CO3
COX7A2
MT-CO1
COX6C
COX7C
COX8A
COX6B1
COX4I1
COX5B
COX6A1
COX5A
COX7B
COX14
COX17
COA3
COX20
COX7A2L
COA4
COA1
COA5
COX19
COX10
COX15
COX4I2
COX6A2
COX6B2
COX7A1
COX7B2
COX8C
CTCs (n=136 cells)
Complex V (n=21)
MT-ATP6
ATP5ME
ATP5MF
ATP5MG
MT-ATP8
ATP5PD
ATP5PF
ATP5F1E
ATP5IF1
ATP5MC3
ATP5PO
ATP5F1B
ATP5MC2
ATP5F1C
ATP5MC1
ATP5PB
ATP5F1D
ATP5F1A
DMAC2L
ATPAF2
ATPAF1
B
Relative expression
3
2
1
0
***
OXPHOS
Glycolysis
FAO
PPP
TCA
Glutamine

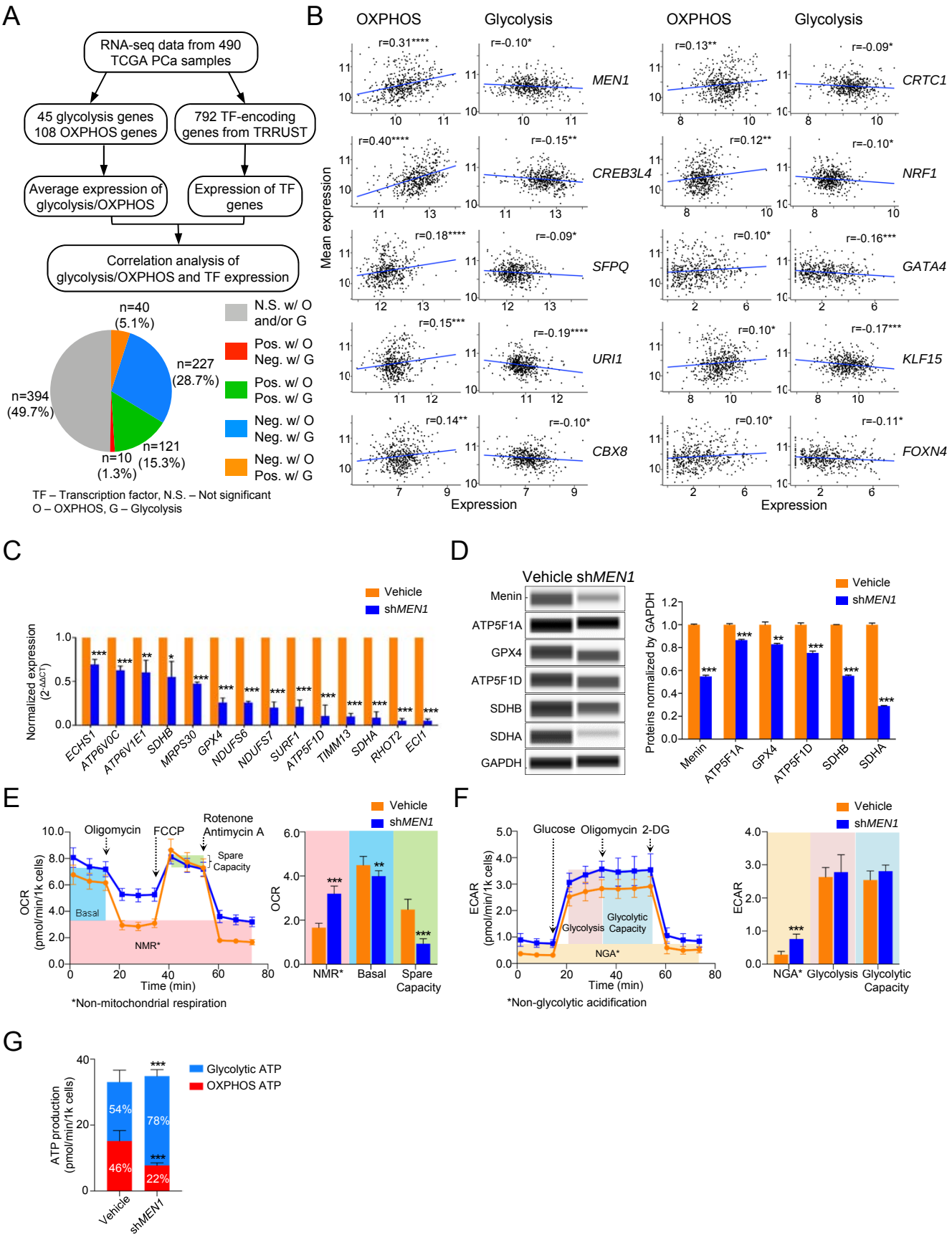
A
RNA-seq data from 490 TCGA PCa samples
45 glycolysis genes 108 OXPHOS genes
792 TF-encoding genes from TRRUST
Average expression of glycolysis/OXPHOS
Expression of TF genes
Correlation analysis of glycolysis/OXPHOS and TF expression
n=40 (5.1%)
n=227 (28.7%)
n=394 (49.7%)
n=121 (15.3%)
n=10 (1.3%)
N.S. w/ O and/or G
Pos. w/ O Neg. w/ G
Pos. w/ O Pos. w/ G
Neg. w/ O Neg. w/ G
Neg. w/ O Pos. w/ G
TF – Transcription factor, N.S. – Not significant
O – OXPHOS, G – Glycolysis
B
OXPHOS
Glycolysis
Mean expression
Expression
MEN1
CREB3L4
SFPQ
URI1
CBX8
CRTC1
NRF1
GATA4
KLF15
FOXN4
C
Vehicle
shMEN1
Normalized expression (2^-ΔΔCT)
ECHS1
ATP6V0C
ATP6V1E1
SDHB
MRPS30
GPX4
NDUFS6
NDUFS7
SURF1
ATP5F1D
TIMM13
SDHA
RHOT2
ECI1
D
Vehicle shMEN1
Menin
ATP5F1A
GPX4
ATP5F1D
SDHB
SDHA
GAPDH
Proteins normalized by GAPDH
E
Oligomycin
FCCP
Rotenone Antimycin A
Spare Capacity
Basal
NMR*
OCR (pmol/min/1k cells)
Time (min)
*Non-mitochondrial respiration
F
Glucose
Oligomycin
2-DG
Glycolysis
Glycolytic Capacity
NGA*
ECAR (pmol/min/1k cells)
Time (min)
*Non-glycolytic acidification
G
Glycolytic ATP
OXPHOS ATP
ATP production (pmol/min/1k cells)
54%
46%
78%
22%
Vehicle
shMEN1

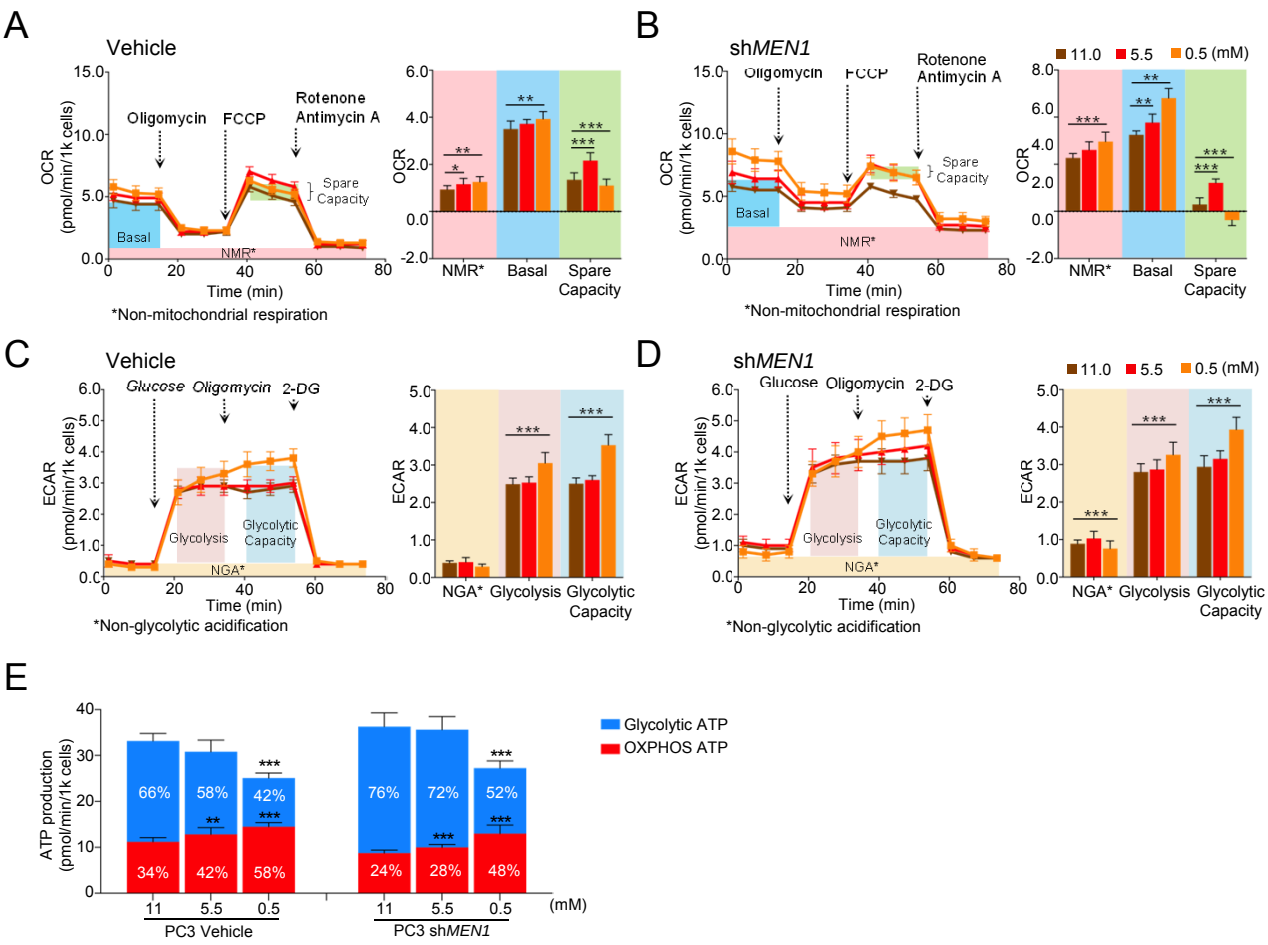
A
Vehicle
OCR (pmol/min/1k cells)
Oligomycin
FCCP
Rotenone
Antimycin A
Spare Capacity
Basal
NMR*
Time (min)
*Non-mitochondrial respiration
NMR*
Basal
Spare Capacity
B
shMEN1
11.0
5.5
0.5 (mM)
C
Vehicle
ECAR (pmol/min/1k cells)
Glucose
Oligomycin
2-DG
Glycolysis
Glycolytic Capacity
NGA*
*Non-glycolytic acidification
NGA*
Glycolysis
Glycolytic Capacity
D
shMEN1
E
ATP production (pmol/min/1k cells)
Glycolytic ATP
OXPHOS ATP
66%
58%
42%
34%
42%
58%
76%
72%
52%
24%
28%
48%
11
5.5
0.5
(mM)
PC3 Vehicle
PC3 shMEN1

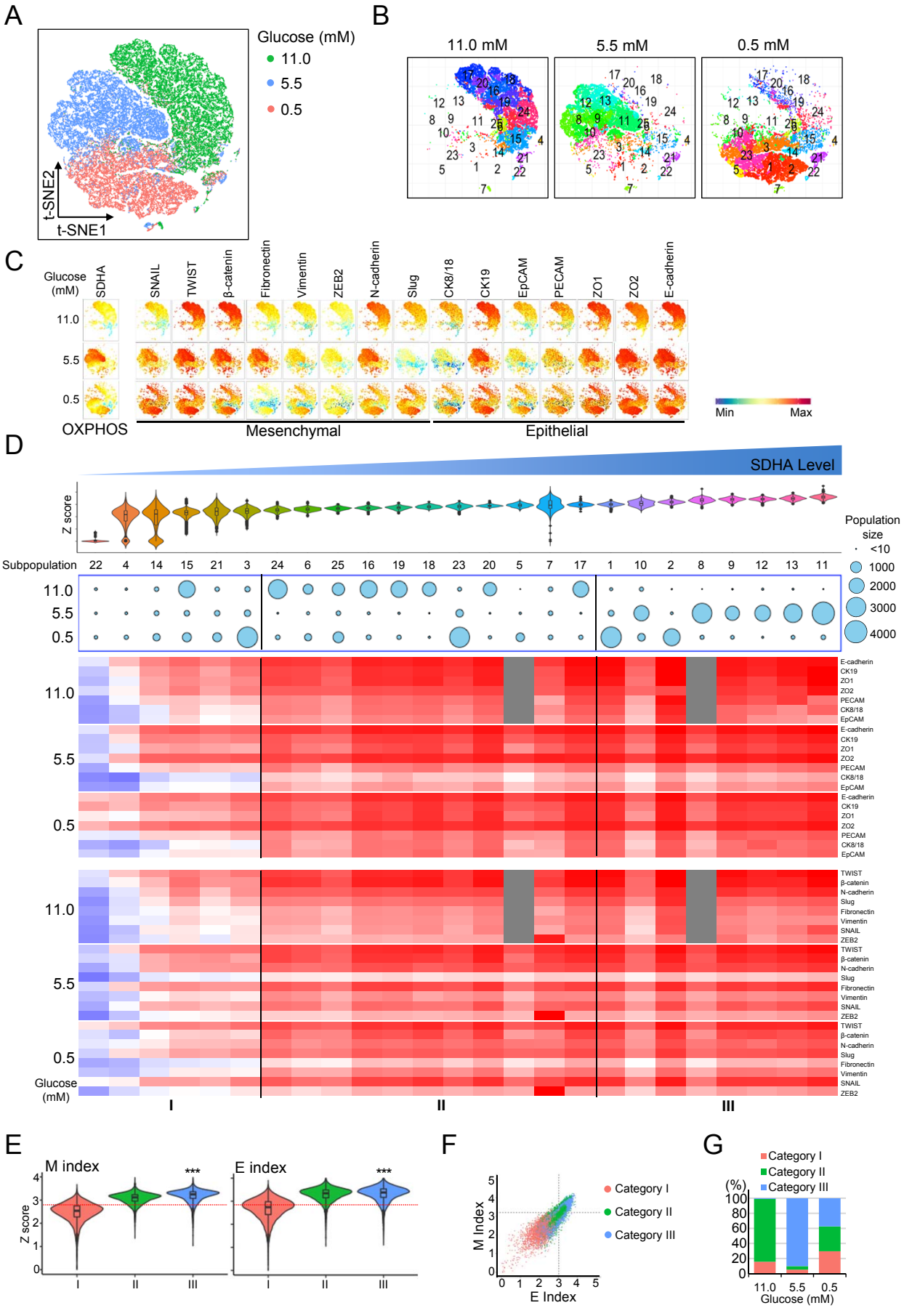
A
Glucose (mM)
11.0
5.5
0.5
t-SNE2
t-SNE1
B
11.0 mM
5.5 mM
0.5 mM
C
Glucose (mM)
SDHA
SNAIL
TWIST
β-catenin
Fibronectin
Vimentin
ZEB2
N-cadherin
Slug
CK8/18
CK19
EpCAM
PECAM
ZO1
ZO2
E-cadherin
OXPHOS
Mesenchymal
Epithelial
Min
Max
D
SDHA Level
Z score
Population size
<10
1000
2000
3000
4000
Subpopulation
22 4 14 15 21 3 24 6 25 16 19 18 23 20 5 7 17 1 10 2 8 9 12 13 11
Glucose (mM)
I
II
III
E
M index
E index
***
Z score
F
M Index
E Index
Category I
Category II
Category III
G
Category I
Category II
Category III
(%)
Glucose (mM)

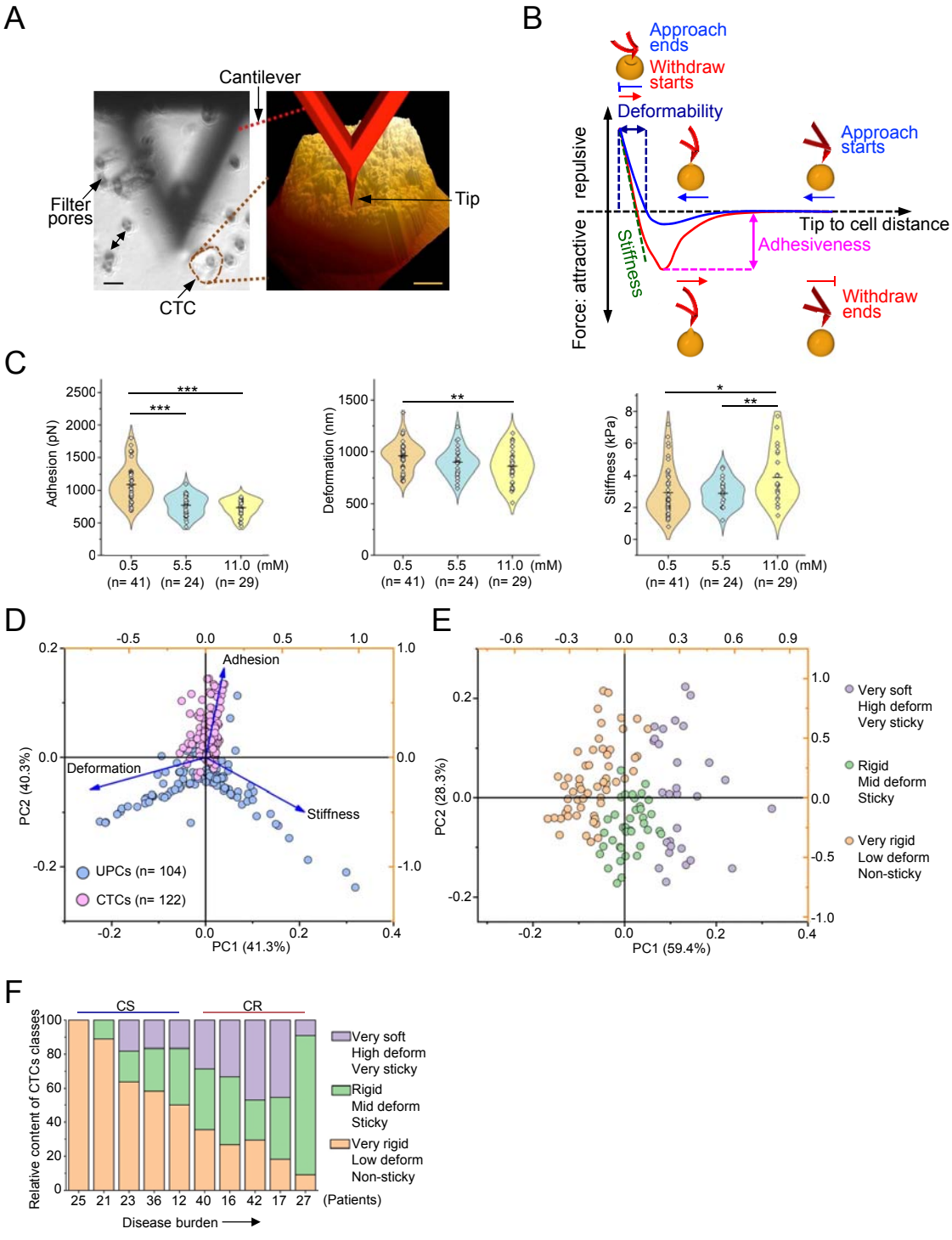
A
Cantilever
Filter pores
Tip
CTC
B
Approach ends
Withdraw starts
Deformability
Approach starts
repulsive
Force: attractive
Stiffness
Tip to cell distance
Adhesiveness
Withdraw ends
C
Adhesion (pN)
Deformation (nm)
Stiffness (kPa)
0.5 5.5 11.0 (mM)
(n= 41) (n= 24) (n= 29)
D
Adhesion
Deformation
Stiffness
UPCs (n= 104)
CTCs (n= 122)
PC1 (41.3%)
PC2 (40.3%)
E
PC1 (59.4%)
PC2 (28.3%)
Very soft
High deform
Very sticky
Rigid
Mid deform
Sticky
Very rigid
Low deform
Non-sticky
F
CS
CR
Relative content of CTCs classes
25 21 23 36 12 40 16 42 17 27 (Patients)
Disease burden

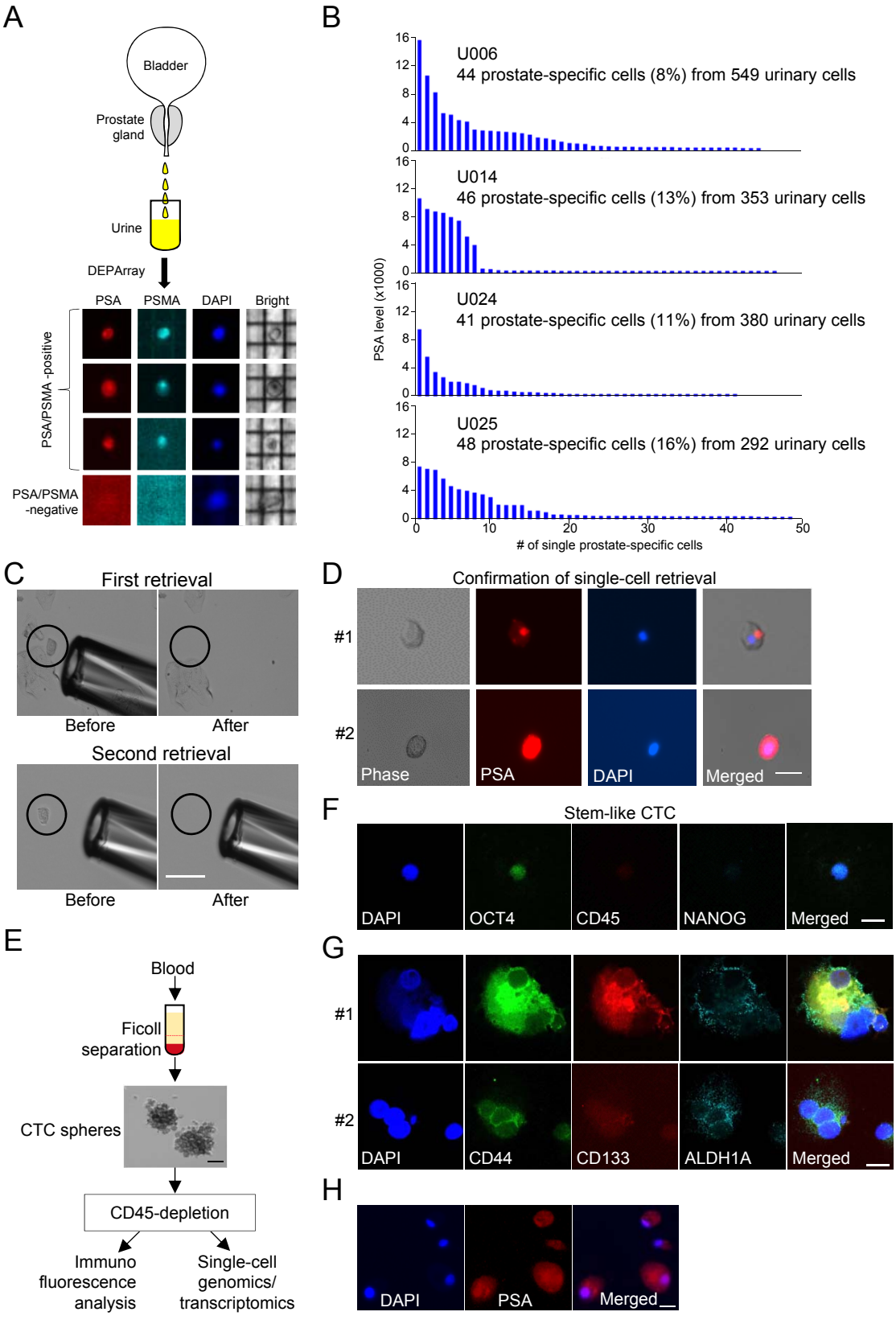
A
Bladder
Prostate gland
Urine
DEPArray
PSA
PSMA
DAPI
Bright
PSA/PSMA -positive
PSA/PSMA -negative
B
U006
44 prostate-specific cells (8%) from 549 urinary cells
U014
46 prostate-specific cells (13%) from 353 urinary cells
U024
41 prostate-specific cells (11%) from 380 urinary cells
U025
48 prostate-specific cells (16%) from 292 urinary cells
PSA level (x1000)
# of single prostate-specific cells
C
First retrieval
Before
After
Second retrieval
Before
After
D
Confirmation of single-cell retrieval
#1
#2
Phase
PSA
DAPI
Merged
E
Blood
Ficoll separation
CTC spheres
CD45-depletion
Immuno fluorescence analysis
Single-cell genomics/ transcriptomics
F
Stem-like CTC
DAPI
OCT4
CD45
NANOG
Merged
G
#1
#2
DAPI
CD44
CD133
ALDH1A
Merged
H
DAPI
PSA
Merged

Figure S1. Isolation and Characterization of Urinary Prostate Cells (UPCs) from Urine Samples and Circulating tumor cells (CTCs) from Blood Samples of Prostate Cancer Patients, Related to Figure 1.

(A) Illustration of urine collection and representative images of PSA/PSMA-positive and -negative cells exfoliated in urine using the DEPArray™ system.
(B) PSA expression shown in fluorescent intensity of UPCs isolated from four patients using DEPArray™.
(C) Examples of single-cell retrieval using a micropipette tip controlled by a micromanipulator. Scale bar, 50 μm.
(D) Representative images of confirmation of retrieved single UPCs with positive PSA immunofluorescence staining. Scale bar, 30 μm.
(E) Schematic processing of CTCs. Scale bar, 50 μm.
(F-G) Immunofluorescence analysis of stem-like CTCs. Examples of an intact cell and cell clusters showing stem-like features. Scale bar, 10 μm.
(H) Example images of CTCs with positive PSA staining. Scale bar, 20 μm.

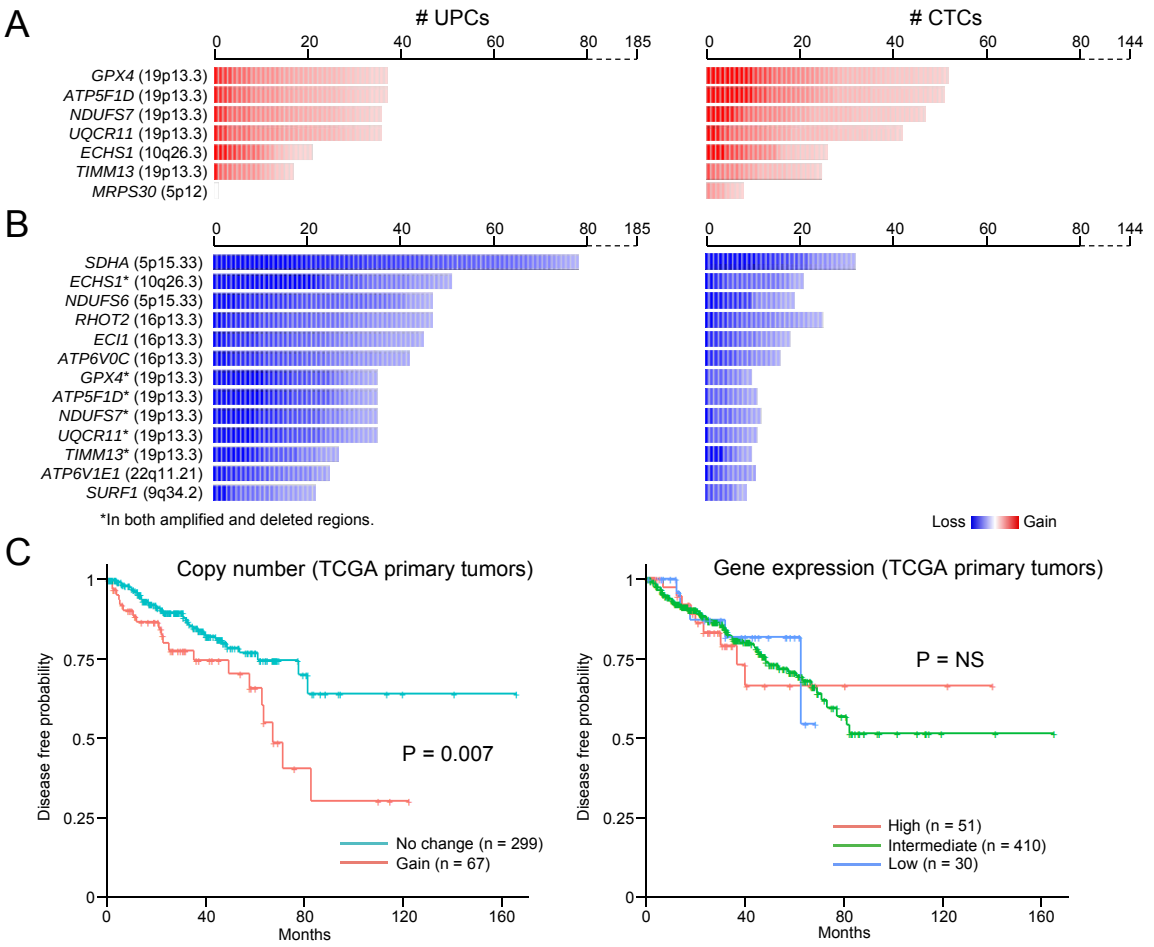

Figure S2. Examples of Genomic Gains and Deletions of OXPHOS Loci in Prostate Cancer, Related to Figure 1.

(A-B) Genomic profiles of the 14 selected OXPHOS loci mapped in the regions that were frequently amplified or infrequently deleted in circulating tumor cells (CTCs) relative to urinary prostate cells (UPCs).
(C) Disease-free survival curves of prostate cancer patients in The Cancer Genome Atlas (TCGA) cohort based on copy number (*left*) and expression levels (*right*) of the 14 mapped OXPHOS loci. Whereas high expression levels of these loci were not a prognosticator for prostate cancer, increased copy-numbers predicted shorter disease-free survival in patients of the TCGA cohort. This implicated that the expression of the 14 OXPHOS genes might not be active in primary tumor cells. However, tumor cells with the pre-existing genomic amplifications may be robustly selected for transcription reprogramming during the blood circulation.

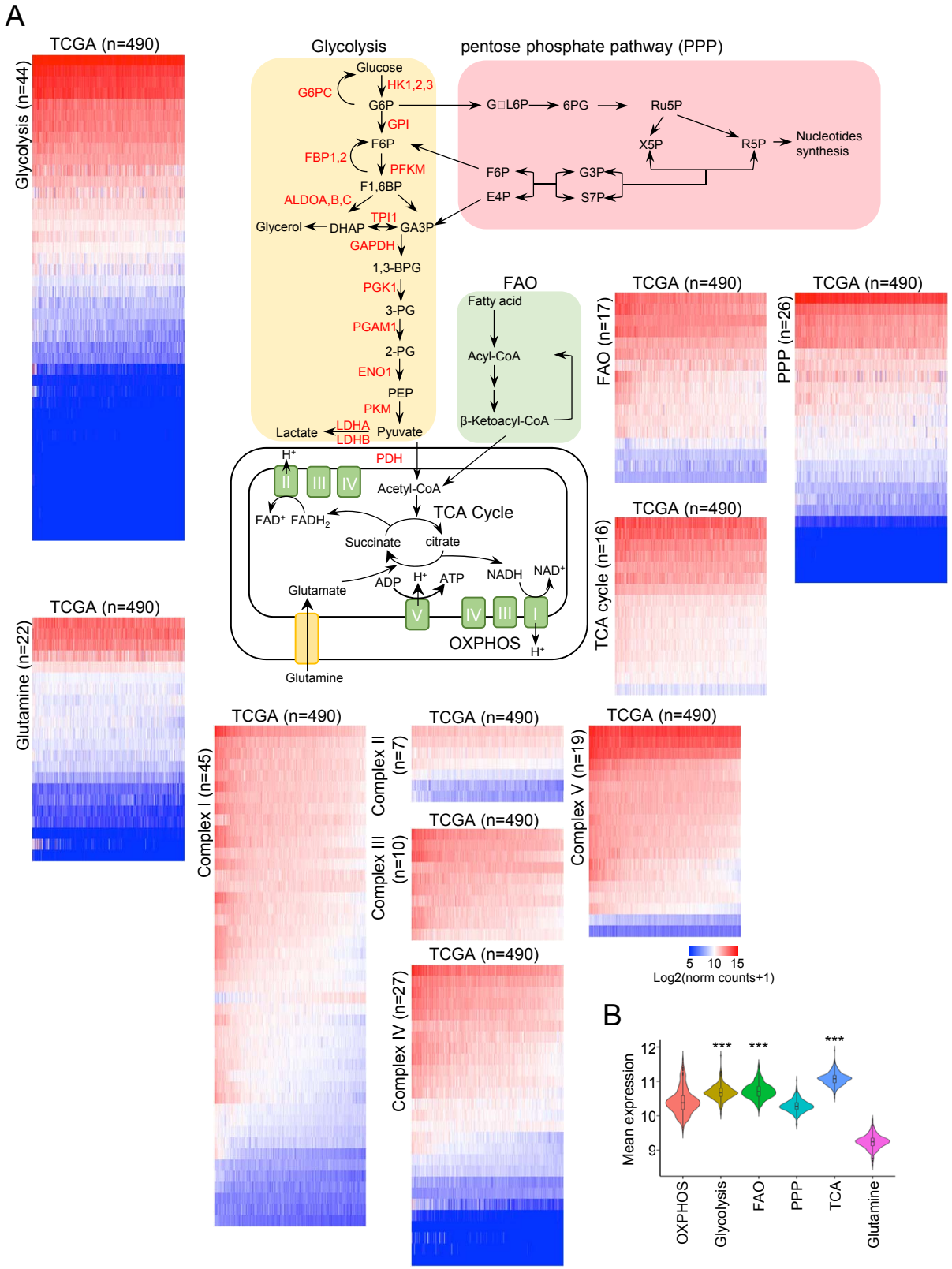
A
TCGA (n=490)
Glycolysis (n=44)
Glycolysis
pentose phosphate pathway (PPP)
Glucose
G6PC
HK1,2,3
G6P
GPI
F6P
FBP1,2
PFKM
F1,6BP
ALDOA,B,C
TPI1
Glycerol
DHAP
GA3P
GAPDH
1,3-BPG
PGK1
3-PG
PGAM1
2-PG
ENO1
PEP
PKM
Lactate
LDHA
LDHB
Pyuvate
G□L6P
6PG
Ru5P
X5P
R5P
Nucleotides synthesis
F6P
G3P
E4P
S7P
FAO
Fatty acid
Acyl-CoA
β-Ketoacyl-CoA
TCGA (n=490)
FAO (n=17)
TCGA (n=490)
PPP (n=26)
PDH
Acetyl-CoA
TCA Cycle
FAD+ FADH2
Succinate
citrate
NADH
NAD+
ADP
ATP
H+
Glutamate
Glutamine
OXPHOS
TCGA (n=490)
TCA cycle (n=16)
TCGA (n=490)
Glutamine (n=22)
TCGA (n=490)
Complex I (n=45)
TCGA (n=490)
Complex II (n=7)
TCGA (n=490)
Complex III (n=10)
TCGA (n=490)
Complex V (n=19)
TCGA (n=490)
Complex IV (n=27)
5 10 15
Log2(norm counts+1)
B
Mean expression
12
11
10
9
***
***
***
OXPHOS
Glycolysis
FAO
PPP
TCA
Glutamine

Figure S3. Expression Profiles of Genes of Metabolic Pathways in the Primary Tumors of The Cancer Genome Atlas (TCGA) Cohort, Related to Figure 2.

(A) Transcriptomic heat maps of genes associated with metabolic pathways including glycolysis, pentose phosphate pathway (PPP), fatty acid oxidation (FAO), TCA cycle, glutamine, and five mitochondrial complexes (OXPHOS).
(B) Violin plots displaying expression level of genes associated with glycolysis, PPP, FAO, TCA cycle, glutamine, and OXPHOS. ***P < 0.001 (Duncan's multiple range test).

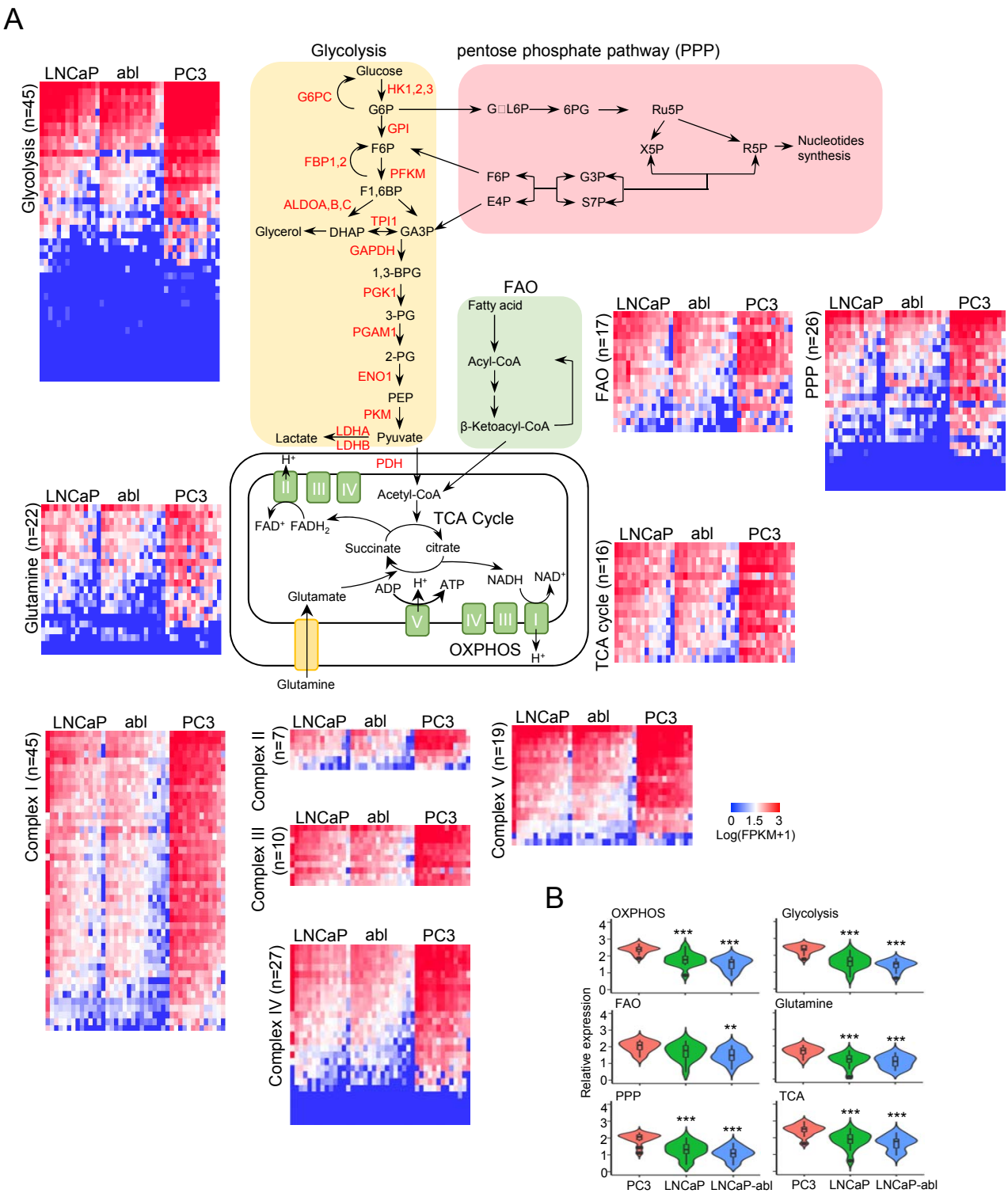

Figure S4. Single-cell Transcriptomic Expression Profiles of Genes of Metabolic Pathways in Prostate Cancer Cell Lines, Related to Figure 3.

(A) Transcriptomic heat maps of metabolic pathways included glycolysis, pentose phosphate pathway (PPP), fatty acid oxidation (FAO), TCA cycle, glutamine, and five complexes of oxidation phosphorylation.

(B) Violin plots displaying expression level of genes associated with glycolysis, PPP, FAO, TCA cycle, glutamine, and OXPHOS. **P < 0.01, ***P < 0.001 (Duncan's multiple range test).

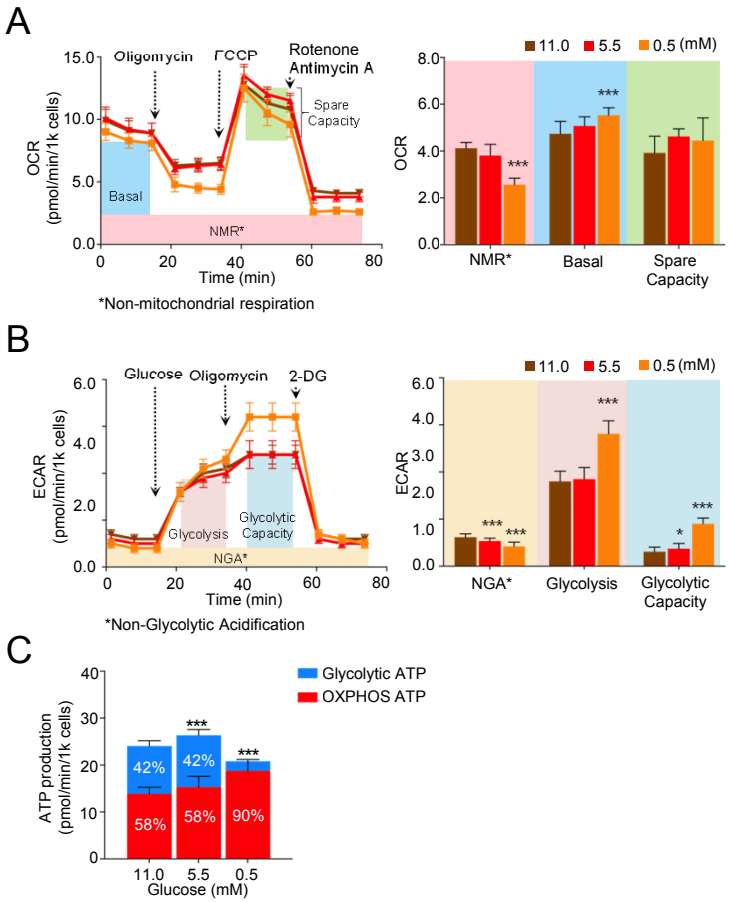

Figure S5. Metabolic Profiles of OXPHOS and Glycolysis in LNCaP Prostate Cancer Cells Cultured in Different Glucose Conditions, Related to Figure 4.

(A) Oxygen consumption rate (OCR) and OXPHOS functional profile of LNCaP cells in 11.0, 5.5 and 0.5 mM glucose conditions.
(B) Extracellular acidification rate (ECAR) and glycolysis profile of LNCaP cells in 11.0, 5.5, and 0.5 mM glucose conditions.
(C) ATP production rates of glycolysis and OXPHOS in LNCaP cells.
*P < 0.05, ***P < 0.001 (Duncan's multiple range test)

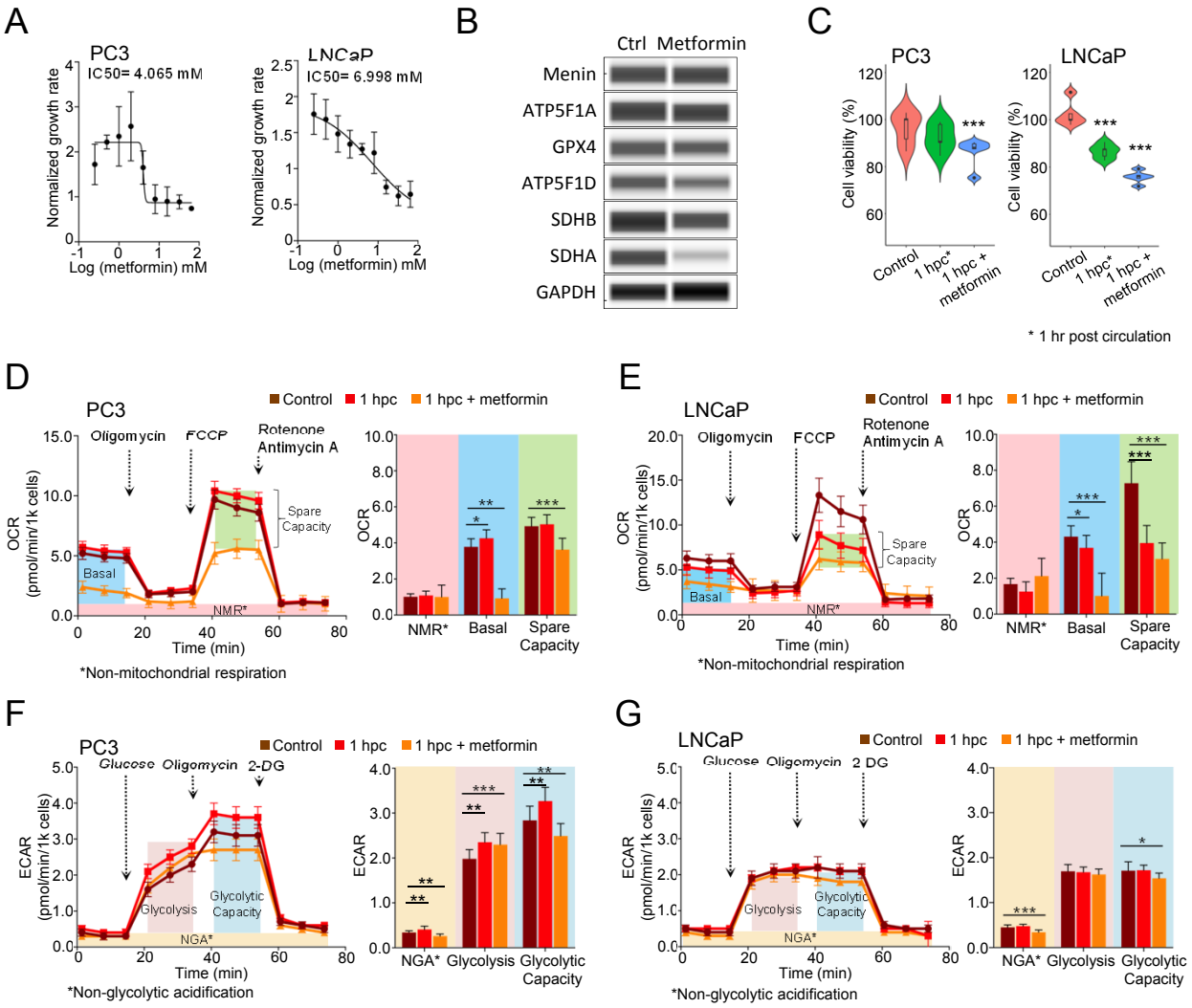

Figure S6. Attenuation of Oxidative Phosphorylation (OXPHOS) Activities by Metformin in an *In Vitro* Circulation Condition, Related to Figure 4.

(A) The half maximal inhibitory concentration (IC50) curves of metformin in PC3 and LNCaP prostate cancer cells. Metformin (4-5 mM) was applied in corresponding assays.
(B) Capillary Western blotting of OXPHOS-related proteins in control and metformin-treated PC3 prostate cancer cells.
(C) Cell viability results of PC3 and LNCaP prostate cancer cells before and after 1 hr in the *in vitro flow assay* with or without metformin treatment. The assay was performed in the ibidi Pump System. Cells were circulated in 5.5 mM glucose culture medium (simulating a blood glucose condition) in the pump system connected with 0.6 mm μ–Slide. The pump system was set up at 16.65 ml/min flow rate to generate 7 dyn/cm^2 shear stress to simulate microvascular wall shear stress.
(D-E) Oxygen consumption rate (OCR) and OXPHOS functional profiles of PC3 and LNCaP prostate cancer cells in control, 1 hr post circulation (hpc), and 1 hpc with metformin. *P < 0.05, **P < 0.01, ***P < 0.001 (Duncan's multiple range test)
(F-G) Extracellular acidification rate (ECAR) and glycolysis functional profiles of PC3 and LNCaP prostate cancer cells in control, 1 hpc, and 1 hpc with metformin. *P < 0.05, **P < 0.01, ***P < 0.001 (Duncan's multiple range test)

Tumor Biology

Abstract 2766: Amplification-associated upregulation of genes involved in oxidative phosphorylation for disseminated prostate cancer cells

Chun-Lin Lin, Tan Xi, Chia-Nung Hung, Pawel A. Osmulski, Chih-Wei Chou, Meizhen Chen, Chiou-Miin Wang, Kohzoh Mitsuya, Nameer Kirma, Maria E. Gaczynska, Chun-Liang Chen, and Tim H.-M. Huang

DOI: 10.1158/1538-7445.AM2019-2766 Published July 2019

Proceedings: AACR Annual Meeting 2019; March 29-April 3, 2019; Atlanta, GA

July 2019
Volume 79, Issue 13
Supplement
Table of Contents

Abstract

Purpose: Little is known about adaptive selection of tumor cells transiting from *in situ* proliferation to distant colonization through blood circulation. This

study used genomic, transcriptomic, and biophysical analyses at single-cell levels to explore biological and physical properties of circulating tumor cells (CTCs) undergoing hemodynamic stress. The aims are trying to understand how CTCs strive to survive in the bloodstream and to develop strategies for therapeutic intervention.

Experimental Design: We compared genomic profiles of CTCs in blood and primary tumor cells shed in urine of prostate cancer patients to identify amplified regions preferentially retained in CTCs. Single-cell RNA-seq was used to confirm amplification-associated overexpression of genes in CTCs.

Results: Among 261 recurrently amplified genomic regions in the analysis, 70 were found predominantly shown in CTCs relative to primary tumor cells. In line with the results at the genomic level, the transcriptomic data of CTCs demonstrate a great amount of cells showing high expression levels in the oxidative phosphorylation (OXPHOS) pathway compared to other hallmark gene sets. The finding suggests that tumor cells with these pre-existing genomic alterations were adaptively selected for transcription reprogramming during blood circulation. Specifically, amplified genes associated with OXPHOS were exploited by CTCs for alternative fuels. As to the upstream of this transcription event, we found the expression of *MEN1*, encoding menin known to form a transcription factor complex with the mixed-lineage leukemia protein (MLL) in prostate cancer cells, was positively correlated with 11 of the 14 OXPHOS loci in the Cancer Genomic Atlas prostate cancer cohort. In vitro assay showed that *MEN1* knockdown by shRNA resulted in attenuation of both mRNA and protein expression of OXPHOS loci in PC-3 cells. Taken together pre-existing amplification of OXPHOS loci can be used as a

transcription apparatus by menin for metabolic reprogramming of tumor cells in response to harsh microenvironments in the bloodstream.

Conclusions: Single-cell profiling identified signaling pathways that are crucial for CTCs to survive in the bloodstream. The finding suggests that a metabolic shift from Warburg to OXPHOS metabolism can be associated with a hybrid mesenchymal-epithelial phenotype of CTCs. Moreover, the study demonstrates the feasibility of routinely conducting single-cell analysis of exfoliated tumor cells for minimally invasive monitoring of disease progression and treatment response in prostate cancer patients

Citation Format: Chun-Lin Lin, Tan Xi, Chia-Nung Hung, Pawel A. Osmulski, Chih-Wei Chou, Meizhen Chen, Chiou-Miin Wang, Kohzoh Mitsuya, Nameer Kirma, Maria E. Gaczynska, Chun-Liang Chen, Tim H.-M. Huang. Amplification-associated upregulation of genes involved in oxidative phosphorylation for disseminated prostate cancer cells [abstract]. In: Proceedings of the American Association for Cancer Research Annual Meeting 2019; 2019 Mar 29-Apr 3; Atlanta, GA. Philadelphia (PA): AACR; Cancer Res 2019;79(13 Suppl):Abstract nr 2766.

Previous

Back to top